Anoctamin8 Tethers the Endoplasmic Reticulum and Plasma Membranes to Assemble Ca^{2+} Signaling Complexes at ER/PM Junctions

Archana Jha[1,4], Woo Young Chung[1,4], Laura Vachel[1], Jozsef Maleth[2], Sarah Lake[1], Guofeng Zhang[3], Malini Ahuja[1] and Shmuel Muallem[1,5]

From [1]The Epithelial Signaling and Transport Section, National Institute of Dental and Craniofacial Research, National Institutes of Health, Bethesda, MD 20892, [2]First Department of Medicine, University of Szeged, Szeged, Hungary, [3]Trans-NIH Shared Resource on Biomedical Engineering and Physical Science (BEPS) National Institute of Biomedical Imaging & Bioengineering.

[4]A.J. and WY.C. are first co-authors.

[5]Address for correspondence:
Shmuel Muallem, Ph.D.
Epithelial Signaling and Transport Section
National Institute of Health,
National Institute of Dental and Craniofacial Research,
Building 10, Room 1N-112, Bethesda MD 20892.
Phone: 301-402-0262
Email: shmuel.muallem@nih.gov

Abstract

Communication and material transfer between membranes and organelles take place at membrane contact sites (MCSs). MCSs between the ER and PM, the ER/PM junctions, are the site where the ER Ca^{2+} sensor STIM1 and the PM Ca^{2+} influx channel Orai1 cluster. MCSs are formed by tether proteins that bridge the opposing membranes, but the identity and role of these tethers in receptor-evoked Ca^{2+} signaling is not well understood. Here we identified ANO8 as a key tether in the formation of the ER/PM junctions that is essential for STIM1-STIM1 and STIM1-Orai1 interaction and channel activation at a $PI(4,5)P_2$-rich domain. Moreover, ANO8 assembles all core Ca^{2+} signaling proteins: Orai1, PMCA, STIM1, IP_3 receptors and SERCA2 at the ER/PM junctions. This controls the efficiency of receptor-stimulated Ca^{2+} signaling and duration of Orai1 activity to prevent Ca^{2+} toxicity. These findings reveal the central role of MCSs in determining efficiency and fidelity of cell signaling.

Running title: ANO8 and Ca^{2+} signaling at the ER/PM junctions

Key words: ANO8/tether/ER/PM contact site/assembly/Ca^{2+} signaling

Introduction

The receptor-evoked Ca^{2+} signal controls virtually all cell functions in all cellular compartments and organelles (Berridge, 2016). The core proteins that form the Ca^{2+} signaling complex include G protein effectors that activate phospholipase C to hydrolyze $PI(4,5)P_2$ and generate IP_3 and diacylglycerol. IP_3 activates the IP_3 receptors (IP_3Rs) in the endoplasmic reticulum (ER) to release Ca^{2+} stored in the ER. Ca^{2+} release from the ER is sensed by the ER Ca^{2+} sensor STIM1, which then clusters at the ER/PM junctions and interacts with and activates the plasma membrane (PM) Ca^{2+} influx channel Orai1 (Berridge, 2016). After the increase in cytoplasmic Ca^{2+} due to ER Ca^{2+} release and PM Ca^{2+} influx, the Ca^{2+} is removed from the cytosol in part by the PM Ca^{2+} ATPase (PMCA) pump and in part by the ER/SR Ca^{2+} ATPase (SERCA) pump. Periodic repeat of this cycle results in physiological Ca^{2+} oscillations (Kiselyov, Wang et al., 2006). Disruption of the cycle by excessive Ca^{2+} influx and sustained increase in cytoplasmic Ca^{2+} is highly toxic (Petersen, 2014). Cells guard against such toxic effects by inhibition of Ca^{2+} influx channels shortly after their activation via fast (FCDI) and slow Ca^{2+}-dependent inhibition (SCDI) (Prakriya & Lewis, 2015), which is mediated by the interaction of Store-operated calcium entry-associated regulatory factor (SARAF) (Jha, Ahuja et al., 2013, Palty, Raveh et al., 2012) and calmodulin (Li, Wu et al., 2017) with STIM1. In addition to these core proteins, the receptor-evoked Ca^{2+} signal is regulated by cytoskeletal proteins (Szasz & Webb, 2017), protein kinases (Jha, Ahuja et al., 2014, Lang, Eylenstein et al., 2012) and lipids (Muallem, Chung et al., 2017).

The many functions mediated by Ca^{2+} require placing the core Ca^{2+} signaling proteins in specific cellular compartments and compartmentalization of the Ca^{2+} signal. Examples of spatial segregation of Ca^{2+} signaling proteins can be seen in spines and synapses (Higley, 2014) and polarized epithelial cells, where all Ca^{2+} signaling proteins are clustered at the apical pole (Hong, Li et al., 2011). Such an arrangement is essential to generate spatially and temporally precise Ca^{2+} signals to modulate specific cellular activity at the site where the Ca^{2+} signal is evoked (Ahuja, Jha et al., 2014, Park, Lomax et al., 2001). It is now clear that compartmentalization of cell signaling is achieved by targeting signaling proteins to membrane contact sites (MCSs) (Chung, Jha et al., 2017, Lahiri, Toulmay et al., 2015, Marchi, Patergnani et al., 2017, Muallem et al., 2017, Nunes-Hasler & Demaurex, 2017). MCSs are formed between the ER and all cellular organelles, including the mitochondria (Marchi et al., 2017) and the PM (Chung et al., 2017, Henne, Liou et al., 2015), by tether proteins. Tether proteins are defined by an ER and target membrane binding motifs that span and bridge the gap between the two membranes.

The best-defined tethers that form the ER/PM MCSs are in yeast, in which the three tricalbins (Toulmay & Prinz, 2012), Ist2 (Maass, Fischer et al., 2009), VAPs (Murphy & Levine, 2016), and a lipid transfer protein are required for formation of ER/PM MCSs (Henne et al., 2015). However ER/PM MCSs in mammalian cells and their role in Ca^{2+} signaling are not well understood. The mammalian homologues of yeast tricalbins are the three Extended Synaptotagmins (E-Syts), which participate in formation of ER/PM MCSs (Giordano, Saheki et al., 2013), but appear to have specific functions. E-Syt1 affects Ca^{2+} signaling (Chang, Hsieh et al., 2013, Maleth, Choi et al., 2014) by regulating translocation of the Orai1-STIM1 to a $PI(4,5)P_2$-rich domain, a function not shared by E-Syt2 and E-Syt3 (Maleth et al., 2014). E-Syt2, but not E-Syt1 or E-Syt3, appears to regulate PI4P and $PI(4,5)P_2$ at the ER/PM junctions (Dickson, Jensen et al., 2016). Recently, GRAMD2a was reported as a junction localized protein that impacts STIM1 clustering, but with no role in Ca^{2+} influx (Besprozvannaya, Dickson et al., 2018). The molecular identity of the mammalian homologue of yeast Ist2 and its role in STIM1-Orai1 function and Ca^{2+} signaling are not known.

Sequence analysis suggests a similarity between Ist2 and members of the Anoctamins family of proteins (Whitlock & Hartzell, 2017). The first two members of the Anoctamin family, ANO1 and ANO2, function as Ca^{2+}-activated Cl^- channels (Stohr, Heisig et al., 2009). ANO6 functions as a lipid scramblase and other Anoctamins have also been found to have some scramblase activity (Whitlock & Hartzell, 2017). The family consists of 10 members, with very limited information on their properties and cellular functions, except for ANO1 (Dang, Feng et al., 2017, Paulino, Kalienkova et al., 2017), ANO2 (Huang, Xiao et al., 2012) and ANO6 (Brunner, Lim et al., 2014, Suzuki, Umeda et al., 2010).

We used knockdown and overexpression strategy to search for an anoctamin that functions as an ER/PM tether controlling STIM1-mediated activation of Orai1 and the subsequent Ca^{2+}-dependent inactivation of Orai1. Of all the anoctamins tested, only Anoctamin 8 (ANO8) fulfills these properties. Silencing of ANO8 reduced STIM1-STIM1 and STIM1-Orai1 interaction in response to store depletion, formation of STIM1 puncta, SOCs-mediated Ca^{2+} influx, activation of Orai1 current and SCDI, while overexpression of ANO8 increased all these parameters. ANO8 mediates a novel mechanism of Orai1 channel inactivation by markedly facilitating SERCA2-mediated Ca^{2+} influx into the ER, an activity antagonized by activation of the IP_3 receptors and chelation of ER Ca^{2+}, even at a Ca^{2+} concentration of 0.2 nM. Furthermore, FRET, Co-IP, and functional analysis revealed that upon cell stimulation ANO8 assembles all the core Ca^{2+} signaling proteins into complexes at the ER/PM junctions, including the ER

STIM1, IP_3Rs and SERCA pumps, and the PM Orai1 and PMCA, thereby regulating all aspects of receptor-evoked Ca^{2+} oscillations. These findings suggest that ANO8 is a key tether that forms ER/PM MCSs to control the fundamental properties of Ca^{2+} signaling.

Results

ANO8 controls STIM1-STIM1 and STIM1-Orai1 interaction at the ER/PM junctions: MCSs are formed by proteins that tether the ER to other cellular membranes and are the sites for the exchange of materials such as lipids and Ca^{2+} ions between membranes and organelles.(Chung et al., 2017, Lahiri et al., 2015, Marchi et al., 2017, Muallem et al., 2017, Nunes-Hasler & Demaurex, 2017). However, the identity of these tethers and their role in cell signaling is poorly understood, particularly in mammalian cells. All forms of cell signaling are initiated at the PM where ligands interact with their receptors, including G protein-coupled receptors that evoke a change in cytoplasmic Ca^{2+}. MCSs at the PM are ER/PM junctions, where STIM1 interacts with and activates Orai1 (Chung et al., 2017, Henne et al., 2015). The only established tethers at the ER/PM junctions to date with a role in Ca^{2+} signaling are the E-Syts (Giordano et al., 2013). Homology analysis suggests that mammalian anoctamins share similarities with the yeast ER/PM tether Ist2. To identify a potential anoctamin that functions as an ER/PM tether we tested the effect of knockdown of ANO1, 2, 3, 5, 8, 9 and overexpression of ANO4, 6, 7, 8 and 10 on STIM1-Orai1 current and slow Ca^{2+}-dependent inactivation (SCDI) of Orai1 current used as a readout of the microdomain localization of STIM1-Orai1 complex (Extended View Fig EV1). Our previous work showed that knockdown of E-Syt1 reduces SCDI (Maleth et al., 2014). Only modification of ANO8 expression affected the current and channel inactivation. Fig 1a shows that expression of ANO8 together with Orai1 and STIM1 increased the rate of SCDI when measured with pipette solution containing the slow Ca^{2+} buffer 3 mM EGTA. Moreover, unlike E-Syt1 which had no effect on current density (Maleth et al., 2014) or Ca^{2+} influx (Giordano et al., 2013), ANO8 also increased current density by 1.39±0.05 fold ($p=0.013$). Furthermore, expression of the yeast Ist2 increased the rate of SCDI and current density, similar to ANO8 (Fig EV2). The increased current, and thus Ca^{2+} at the junctions, can account for the increase in SCDI observed with ANO8. However, Fig 1b shows that the increased SCDI by ANO8 was reduced by knockdown of SARAF, suggesting that ANO8 affects the function of SARAF at the ER/PM junction (Maleth et al., 2014). Expression of ANO8 increased the native SOCs activated by passive ER Ca^{2+} store depletion due to inhibition of the SERCA pumps (Fig 1c).

Fig 1b shows that SARAF mediated part of the SCDI measured in the presence of ANO8 in pipette solution buffered with the weak Ca^{2+} buffer EGTA. FRET was then used to directly examine association of ANO8 with STIM1, Orai1 and SARAF. Figs. 1d and 1f show basal FRET between STIM1 and ANO8 and an increase in FRET upon store depletion. However, there was minimal FRET between Orai1 and ANO8, and no increase in FRET even when YFP-ANO8 and mCherry-Orai1 are co-expressed with myc-STIM1 (Fig EV3a). Moreover, ANO8 had no effect on the current of constitutively active Orai1(V102C) mutant (Fig EV3b). SARAF interacts with STIM1 only in the presence of Orai1 (Maleth et al., 2014). Accordingly, STIM1 and SARAF showed no increased interaction in response to store depletion in the absence of Orai1 (black trace in Fig 1e). However, co-expression of ANO8 was sufficient to increase interaction of STIM1 and SARAF upon store depletion, even in the absence of Orai1 (red trace in Fig 1e). These findings indicate that ANO8 enhances access of SARAF to STIM1 likely in the ER/PM junctions, since SARAF interacts with STIM1 only when STIM1 is in the ER/PM junctions (Maleth et al., 2014).

To further examine the relationship between STIM1 and ANO8, we first determined their localization by confocal microscopy. Fig EV4a shows that in resting cells ANO8 showed mostly ER expression pattern and co-localized with STIM1. Store depletion resulted in translocation of significant portion of ANO8 to the PM (Fig EV4b). To determine whether ANO8 interacts and affects STIM1 while still in the ER, we measured by FRET the effect of ANO8 on STIM1-STIM1 interaction. In resting cell overexpression of ANO8 had minimal effect on STIM1-STIM1 interaction (Fig 1g). Notably, ANO8 significantly increases STIM1-STIM1 interaction, while knockdown of ANO8 reduced STIM1-STIM1 interaction in response to store depletion (Fig 1g). These somewhat unexpected results were confirmed by an independent Co-IP assay in Fig 1h, which shows that ANO8 increased STIM1-STIM1 Co-IP while knockdown of ANO8 markedly reduced STIM1-STIM1 interaction in resting cells (R) and in response to cell stimulation (S). The impact of ANO8 on STIM1-Orai1 interaction was examined by several assays. Fig 1i shows that ANO8 increased FRET between STIM1-Orai1. Analysis by TIRF microscopy showed co-clustering of STIM1, Orai1, and ANO8 at the junctions in response to store depletion (Fig 1j). ANO8 increased both the rate and the number of STIM1 puncta (Fig 1k-m) and Orai1 puncta (Fig 1n) at the ER/PM junctions by about 50%. Additional evidence for the role of native and expressed ANO8 in STIM1-Orai1 interaction was obtained by Co-IP. Immunoprecipitation (IP) of native ANO8 (A8) Co-IPed STIM1 in resting cells, which tended to increase by cell stimulation (Fig 2a), although the effect of cell stimulation did not reach statistical significance, probably due to the quality of the antibodies. A clear effect of knockdown of ANO8 is shown in Fig 2b, in which siANO8 eliminated the native STIM1-Orai1 interaction in response to store depletion.

Effect of ANO8 of STIM1-Orai1 Co-IP was readily observed with the overexpressed proteins (Fig 2c).

ANO8 functions as a tether at the ER/PM junctions*:* The effect of ANO8 on native and expressed STIM1-Orai1 interaction raised the question if all effects of ANO8 are due to its impact on STIM1-STIM1 interaction. To address this question, we tested the effect of ANO8 on the PM level of STIM1-Orai1 complexes. Since only 40% of Orai1 is at the PM at steady-state and store depletion traps part of Orai1 at the ER/PM junctions (Hodeify, Selvaraj et al., 2015), we reasoned that increased STIM1-STIM1 interaction at the ER by ANO8 should not affect surface membrane Orai1 and STIM1. On the other hand, increased level of STIM1 and Orai1 at the PM would suggest effect of ANO8 on the junctions. The results in Figs. 2d-g indicate that ANO8 increased the PM level of Orai1 (Fig 2e) and its interaction with STIM1 (Fig 2f) in the resting state, with additional increase in response to store-depletion. ANO8 was found in the STIM1-Orai1 complex in the resting state and additional ANO8 was recruited to the complex by store depletion (Fig 2g). Constitutively active STIM1 mutants are maximally clustered independent of store depletion and should not be affected by the effect of ANO8 on STIM1-STIM1 interaction. Any effect of ANO8 on their clustering should be due to effect of ANO8 on the ER/PM junctions. We used three constitutively active STIM1 mutants, STIM1(D76A) (Liou, Kim et al., 2005), STIM1-Kras (Maleth et al., 2014) and STIM1(ΔCTID) (Jha et al., 2013), all of which are in the junction independent of store depletion. Figs. S5 shows that knockdown of ANO8 reduced the clustering of STIM1(D76A) (Figs. S5a-c) and the Orai1 current density and SCDI by STIM1-Kras (Fig EV5d,e). Knockdown of ANO8 reduced current by STIM1(ΔCTID), even when measured at 10 mM BAPTA that minimized Ca^{2+}-dependent channel inactivation (Fig EV5f,g). Finally, to obtain independent and direct evidence that ANO8 controls the ER/PM junctions, we analyzed the junctions by electron microscopy (EM). Fig 2h shows example EM images and Fig 2i shows analysis of the size and number of junctions in cells transfected with empty vector (Con) and with ANO8. It is clear that ANO8 increased the size of the ER/PM junctions.

Because ANO8 knockdown prominently reduced STIM1-STIM1 and STIM1-Orai1 interaction and Orai1-STIM1 complexes at the plasma membrane, we measured the effect of knockdown of ANO8 on Orai1 current, native Ca^{2+} influx, and STIM1 clustering. Figs 3a and 3b show that knockdown of ANO8 prominently reduced Orai1 current by about 70% without changing channel inward rectification. Similarly, knockdown of ANO8 reduced the native store-operated Ca^{2+} influx by about 50% (Fig 3c). This inhibition appears to be due to reduced STIM1 puncta at the TIRF plane by about 50% (Figs 3d, e). Together, the findings in Figs 1-3 and and S5 indicate that ANO8 modulates clustering of STIM1 and the assembly and interaction of STIM1 and Orai1 at

the ER/PM junctions, which in turn regulate the activation of Orai1 by STIM1 and the duration of Ca^{2+} influx, as expected from a *bona fide* ER/PM tether.

Novel ANO8-mediated, slow SARAF-independent Orai1 inactivation (SSII) at very low cytoplasmic Ca^{2+}: The current measurement in Figs 1a and 3a was performed with pipette solution containing the slow Ca^{2+} buffer 3 mM EGTA, a concentration at which both fast and slow Ca^{2+}-dependent current inactivation are maximal. To evaluate the effect of ANO8 on the current while minimizing inactivation we measured the current using pipette solution containing 10 mM of the fast Ca^{2+} buffer BAPTA and no added Ca^{2+}, with a calculated global free Ca^{2+} concentration of about 0.2 nM (assuming at most 10 µM total Ca^{2+} in pipette solution mainly due to contaminant in the Cs^{+}-methanosulfonate salt). In this condition, fast and slow Ca^{2+}-dependent current inactivation is minimal, if it occurs at all (Prakriya & Lewis, 2015). Interestingly, Fig 3f shows that with 10 mM BAPTA in the pipette ANO8 still increased STIM1-activated Orai1 current by about 60%. Moreover, unexpectedly, the current in the presence of ANO8 slowly inactivated despite the high concentration of BAPTA that prevented the SCDI in the absence of ANO8 (compare black traces in Figs. 3a and 3f). This form of slow inactivation was independent of SARAF action. Fig 3h shows no SCDI in the presence of 10 mM BAPTA and in the presence and absence of SARAF, while Fig 3i shows that ANO8-dependent slow inactivation is not reduced by knockdown of SARAF.

The Anoctamin family proteins have a highly conserved Ca^{2+} binding site (Brunner et al., 2014, Dang et al., 2017, Paulino et al., 2017) which is also present in ANO8 (Fig EV6a). Mutations of the residues that form the Ca^{2+} binding site shift the Ca^{2+}-dependent activation of ANO1 Cl^{-} current from 0.36 µM to as high as 2 mM (Brunner et al., 2014, Dang et al., 2017, Paulino et al., 2017). On the other hand, ANO8 increased the current with 3 mM EGTA or 10 mM BAPTA in pipette solution and Ca^{2+} influx at cytoplasmic Ca^{2+} concentration of 100 nM in native cells, suggesting that the ANO8 Ca^{2+} binding site does not affect the tethering function of ANO8. Accordingly, Figs S6b,c show that mutating two key residues in the Ca^{2+} binding site of ANO8 had no effect on ANO8-mediated increase in Orai1 current density and ANO8-dependent slow SSII.

ANO8 function depends on PM $PI(4,5)P_2$: Tethers require ER and PM anchors. ANO8 is anchored at the ER (Fig EV4) and should have a PM interacting site. A typical PM anchor is $PI(4,5)P_2$ and the ANO8 yeast homologue Ist2 has a C terminus $PI(4,5)P_2$ binding site (Maass et al., 2009). In addition, the activity of ANO1 (De Jesus-Perez, Cruz-Rangel et al., 2018) and ANO6 (Aoun, Hayashi et al., 2016, Ye, Han et al., 2018) is regulated by $PI(4,5)P_2$, which

prevents channel rundown (De Jesus-Perez et al., 2018, Ye et al., 2018). Therefore, we first determined if the function of ANO8 requires PM $PI(4,5)P_2$ by depleting $PI(4,5)P_2$ with PM targeted 5'-phosphatase (Korzeniowski, Popovic et al., 2009). Figs 4a-c show that $PI(4,5)P_2$ depletion eliminated the ANO8-dependent increase in Orai1 current and SSII and reduced accumulation of ANO8 at the junctions in response to store depletion. Further evidence for the role of $PI(4,5)P_2$ in the function of ANO8 was obtained by testing the effect of ANO8 on STIM1(ΔK). Interaction of the STIM1 polybasic domain with $PI(4,5)P_2$ is required for clustering at the ER/PM junctions (Liou, Fivaz et al., 2007, Maleth et al., 2014). STIM1(ΔK) can activate Orai1, but only when expressed at high levels and in a $PI(4,5)P_2$-poor domain (Maleth et al., 2014). Fig EV7a shows that expression of STIM1(ΔK) at low levels poorly activated Orai1. ANO8 markedly increased Orai1 current activated by STIM1(ΔK) and revealed the SSII. This was due to recruitment of STIM1(ΔK) to $PI(4,5)P_2$ at the ER/PM junctions, since ANO8 increased clustering of STIM1(ΔK) (Fig EV7b,c) and deletion of $PI(4,5)P_2$ eliminated activation of STIM1(ΔK) by ANO8 (Fig EV7d).

Regulation of ANO6 by $PI(4,5)P_2$ (Aoun et al., 2016, Ye et al., 2018) was suggested to be by positively charged sequence (Ye et al., 2018), which is not conserved in other anoctamins, including ANO8. We searched for potential PM phospholipid binding sites at the ANO8 N and C termini using the BHsearch program (http://helixweb.nih.gov/bhsearch) (Brzeska, Guag et al., 2010). The sites identified with the highest scores are shown in red in Fig EV8. Although deletion of the first 20 and 50 residues of ANO8, which includes the RGKR and KLFGKRLLQAGR sites, eliminated the effect of ANO8 on the current and on SSII, mutation of R and K in RGKR and first K and KR individually or together had no effect on the increased current and SSII. The first predicted C terminus $PI(4,5)P_2$ interacting sites (RREAFKR) is close to the last TMD that ends at D861 and cannot access the PM. The mouse ^{1011}PRPGKL^{1016} motif is not conserved in human ANO8. Mutation of the RRR underlined in ^{948}RPRRP^{952} eliminated activation of Orai1 and the SSII by ANO8 (Fig 4d) and accumulation of $ANO8^{R948,950,951Q}$ at the ER/PM junctions in response to store depletion (Fig 5e). Together, the findings in Figs 4, and S7 suggest that ANO8 interacts with $PI(4,5)P_2$ at the PM.

SSII is mediated by SERCA2: Plotting the inactivation slope as a function of the size of the current provided a clue about the mechanism mediating the prominent ANO8-dependent SSII observed in the presence of 10 mM BAPTA. The current was measured at similar STIM1/Orai1 transfection with and without ANO8 by varying external Ca^{2+} between 2-50 mM. Fig 5a shows that ANO8 increased this relationship by almost 4-fold. The size of the current is expected to determine the Ca^{2+} concentration at the ER/PM junctions with ANO8 increasing the local Ca^{2+} at

the junction. This prediction was tested by measuring the effect of ANO8 on fast Ca^{2+}-dependent inactivation (FCDI) of Orai1 that is primarily determined by Ca^{2+} concentration at the mouth of Orai1 (Parekh, 2017, Prakriya & Lewis, 2015). Figs. S9a, and S9b show that ANO8 increased FCDI when compared at the same Orai1 current in cells with and without ANO8. Fitting the inactivation to two exponentials shows that this is primarily by increasing the first time constant (Fig EV9b).

The increase in junctional Ca^{2+} by ANO8 suggested that ANO8 increased the activity of a Ca^{2+}-dependent process that can inactivate the Orai1 current. Such a process can be mediated by SERCA2, which by reloading the ER with Ca^{2+} can reduce the current. We used two independent assays to test this possibility. Figs 5b,c show that inhibition of SERCA2 with CPA in cells that do not express ANO8 and buffered with 3 mM EGTA or 10 mM BAPTA had a small effect on the rate and extent of current inactivation. By contrast, Figs 5d,e show that inhibition of SERCA2 with CPA markedly inhibited the ANO8-dependent SSII in cells buffered with EGTA or BAPTA. If SSII is due to reuptake and accumulation of Ca^{2+} in the ER, then reducing ER Ca^{2+} accumulation should also reduce SSII. To this end, we included 100 μM IP_3 and 10 mM TPEN in the pipette solution. High concentration of IP_3 was used to allow some activation of the IP_3 receptors (IP_3Rs) in the presence of such low Ca^{2+} of 0.2 nM (Mak & Foskett, 2015). Figs 5f,g show that SSII was considerably reduced by IP_3, particularly during the first 2 min of current measurement. SSII resumed after about 2 min, likely due to inactivation of the IP_3Rs at the low cytoplasmic Ca^{2+}, allowing ER Ca^{2+} accumulation by SERCA2. TPEN chelates and prevents accumulation of Ca^{2+} in the ER (Hofer, Fasolato et al., 1998). Figs 5f,g show that SSII was strongly reduced by including 10 mM TPEN in the pipette solution.

A second protocol used to examine the role of SERCA2 in SSII was measuring the effect of ANO8 on the rate of Ca^{2+} uptake into the ER by measuring Ca^{2+} content in the ER with ER-GECO1 (Figs 6a-6d). ER Ca^{2+} was first depleted by stimulating cells in Ca^{2+}-free solution expressing M3 receptors in the presence of high concentrations of carbachol. The stimulated state was then inhibited with atropine, and then the ER was reloaded by exposing the cells to a solution containing 5 mM Ca^{2+}. ER Ca^{2+} uptake was analyzed in the cells' periphery (panel a) and the cells' center (panel b). The traces in expanded time scale and the summary in Fig 6c show that ANO8 increased the rate of Ca^{2+} uptake primarily by the peripheral ER. These findings together with the findings in Fig 5, suggest that ANO8 may recruit the SERCA2 pumps to the ER/PM junctions. This is supported by multiple findings in Figs 6e-6g. Fig 6e shows that ANO8 increases the Co-IP of the native STIM1 and SERCA2 and Fig 6f shows similar findings with the expressed proteins. The FRET measurements in Fig 6g show that store depletion

increased the interaction between STIM1-CFP and SERCA2-YFP, and ANO8 prominently increased this interaction.

ANO8 assembles Ca^{2+} signaling complexes at the ER/PM junctions to control Ca^{2+} signaling: While measuring ER Ca^{2+} depletion in response to receptor stimulation in Fig 6a,b we found that ANO8 markedly increased this rate. The averages in Fig 6d show that ANO8 primarily increased the rate of ER Ca^{2+} depletion in the cell periphery. ER Ca^{2+} release is mediated by receptor-stimulated IP_3 production and activation of the IP_3Rs. To determine whether ANO8 affects IP_3 production, we used the GFP-tagged PLCδ PH domain ($PH_{PLC\delta}$-GFP) to measure PM $PI(4,5)P_2$ and mCherry-ER-GECO1 to simultaneously measure ER Ca^{2+} content. Figs 6h,i show that ANO8 similarly increased the rates of IP_3 production and ER Ca^{2+} release. In addition, Fig 6j shows that ANO8 enhanced the Co-IP of the native STIM1 and IP_3Rs and Fig 6k shows that ANO8 increased the FRET between STIM1-YFP and IP_3R3-mCherry, suggesting that ANO8 enhances recruitment of IP_3 receptors to the ER/PM junctions at which STIM1-Orai1 cluster. Another core component of the Ca^{2+} signaling complex is PMCA. The Co-IP experiments in Fig 6f and the FRET experiments with STIM1-YFP and PMCA-mCherry in Fig 6l show that PMCA is also recruited to the ER/PM junctions.

The results in Figs 1-3, and 6 indicate that all core Ca^{2+} signaling proteins are assembled into complexes at the ER/PM junctions upon cell stimulation with the aid of tether proteins, with ANO8 playing a primary role in the assembly. To test the physiological significance of ANO8-mediated clustering of Ca^{2+} signaling proteins we measured receptor-stimulated physiological Ca^{2+} oscillations. Figs 7a-d show that overexpression of ANO8 alone with native level of all other Ca^{2+} signaling proteins was sufficient to increase the number of responding cells and the frequency and amplitude of the oscillations. Conversely, Figs 7e-h show that knockdown of ANO8 reduced all parameters of the receptor-evoked Ca^{2+} signaling.

Discussion

Information and material flow between cellular compartments and organelles must occur with high fidelity to ensure coordination among all cellular processes. For faithful information flow, cells use membrane contact sites (MCSs) between the ER that spans the entire cell interior and all other cellular membranes (Chung et al., 2017, Lahiri et al., 2015, Marchi et al., 2017, Muallem et al., 2017, Nunes-Hasler & Demaurex, 2017). MCSs are formed by tether proteins that are anchored in the ER, either directly or through VAP proteins (Murphy & Levine, 2016), with cytoplasmic domains that span the distance between the ER and the target

membranes they interact with (Muallem et al., 2017). These features are present in the ER/PM junction tethers E-Syts (Giordano et al., 2013), GRAM domain proteins (Besprozvannaya et al., 2018) and the yeast Ist2 (Maass et al., 2009). The present studies show that ANO8 fulfills all the criteria for a tether and functions as a tether at the ER/PM junctions. Similar to other ANO family members and its yeast homologue Ist2, ANO8 is predicted to have 10 TMD, is located in the ER, and has a long cytoplasmic C terminus rich in basic residues that has putative $PI(4,5)P_2$ interacting motifs (Figs. 4, S4 and S7).

ANO8 tether the ER/PM junctions and translocates to the junctions in response to store depletion. Moreover, importantly, ANO8 increases the number of puncta and rate of puncta formation, indicating that ANO8 actively participates in the assembly of STIM1-Orai1 complexes (and other Ca^{2+} signaling proteins) at the ER/PM junctions. ANO8 accomplish this by promoting both STIM1-STIM1 interaction in response to store depletion (Fig 1g, h) and ER/PM junctions size (Fig 2h, i). Interaction and clustering of STIM1-STIM1 is believed to require the open conformation of STIM1 in which the CC1 and CTID domain are not in contact with the SOAR domain (Jha et al., 2013, Muik, Fahrner et al., 2011, Stathopulos, Schindl et al., 2013). ANO8 can facilitate STIM1-STIM1 interaction by binding to STIM1 in the ER to initiate the STIM1 open conformation. However, it is also possible that by expanding the ER/PM junctions ANO8 facilitates translocation of STIM1 to the junctions, which is sufficient for STIM1-STIM1 interaction. However, this STIM1-STIM1 interaction is not sufficient for stabilization of STIM1 at the junctions since ANO8 only minimally increases STIM1 puncta in the TIRF plane before Ca^{2+} store depletion. Irrespective of the exact mechanism by which ANO8 facilitates STIM1-STIM1 interaction, ANO8 appears to play a critical role in Ca^{2+} signaling than that played by the other ER/PM junction tethers: E-Syts and GRAM domain proteins. Analysis of Ca^{2+} signaling and CRAC current by the showed that E-Syt1 has a minimal role in Ca^{2+} signaling (Chang et al., 2013, Giordano et al., 2013, Maleth et al., 2014) and mainly affects translocation of STIM1-Orai1 complexes to a high $PI(4,5)P_2$ domain without affecting current density (Maleth et al., 2014). By contrast, ANO8 function is essential for CRAC current, Ca^{2+} influx, and the receptor-evoked Ca^{2+} signal.

Intracellular Ca^{2+} is essential for life and death, with physiological Ca^{2+} concentrations mediating numerous essential cellular functions, while high sustained cytoplasmic Ca^{2+} increase causes cell toxicity and death (Berridge, 2016, Petersen, 2014, Prakriya & Lewis, 2015). The cause of high sustained cytoplasmic Ca^{2+} is excessive Ca^{2+} influx, mainly through SOC channels (Prakriya & Lewis, 2015). Inactivation of the Ca^{2+} influx channels shortly after their activation is an important protective mechanism against excessive Ca^{2+} influx and cell toxicity

(Parekh, 2017, Prakriya & Lewis, 2015). Two well-established protective mechanisms are the fast and slow Ca^{2+}-dependent inactivation of the Orai1-STIM1 current that are mediated by a STIM1 negatively charge sequence (Derler, Fahrner et al., 2009, Lee, Yuan et al., 2009, Mullins, Park et al., 2009) within the STIM1 CTID domain (Jha et al., 2013). Two proteins appear to mediate the inactivation: SARAF (Maleth et al., 2014, Palty et al., 2012), which mediates both the fast and slow inactivation (Maleth et al., 2014), and calmodulin (CaM), recently shown to affect SCDI by causing dissociation of STIM1 oligomers (Li et al., 2017). Notably, deletion of SARAF (Maleth et al., 2014) and inhibition of $[Ca^{2+}]_m$ (Li et al., 2017) inhibit SCDI by only about 50%, indicating the involvement of another prominent inactivation mechanism. The present study reveals a novel mechanism in which recruitment of SERCA2 pumps to the ER/PM junction initiates Ca^{2+} uptake specifically into the junctional ER. Ca^{2+} uptake into the junctional ER mediates a substantial part of the slow Ca^{2+}-dependent inactivation.

SERCA2-mediated Ca^{2+} uptake into the ER outside the junctional (peripheral) ER was not affected appreciably by ANO8 even in fully store-depleted cells, suggesting that the junctional ER behaves differently than the ER in other part of the cells. This implies that the junctional ER is functionally segregated from the bulk ER to allow regulation of the Ca^{2+} influx channels activity. Compartmentalization of the ER is also suggested by the quantal properties of IP_3-mediated Ca^{2+} release (Muallem, Pandol et al., 1989, Shin, Luo et al., 2001). Ca^{2+} uptake by peripheral SERCA2b was observed when cytoplasmic Ca^{2+} was buffered to or below 0.2 nM. However, SERCA2b apparent affinity for Ca^{2+} is about 0.44 μM with no uptake observed at Ca^{2+} concentrations below 10 nM (Lytton, Westlin et al., 1992). Therefore, it is likely that the junctional SERCA2b pumps experience Ca^{2+} concentration higher than 0.2 nM due to their localization in close proximity to Orai1 at the ER/PM junctions. This is supported by the findings that ANO8 increases that FCDI (Fig EV9) that depends on local Ca^{2+} at the mouth of Orai1 (Parekh, 2017). Thus, ANO8 recruits SERCA2 pumps to the junctions to facilitate Ca^{2+} uptake by the junctional ER, restricting Ca^{2+} influx and guarding against Ca^{2+} toxicity.

ANO8 promotes assembly of all core Ca^{2+} signaling proteins at the ER/PM junctions to control the receptor-evoked Ca^{2+} signal and Ca^{2+} oscillations. The FRET and Co-IP measurements suggest that ANO8 increases spatial proximity of the Ca^{2+} signaling proteins to tighten the complexes. TIRF and surface expression measurements suggest that ANO8 also increases the number of Ca^{2+} signaling complexes at the junctions by increasing the steady-state level of Orai1 in the PM and the junctions. The result is an increase in all parameters of receptor-evoked Ca^{2+} oscillations, indicating an increase signaling responsiveness and fidelity.

Therefore, the present work reveals that an important function of tether proteins is to increase efficiency and precession of cell signaling and communication between cellular compartments. Disruption of the localization of signaling complexes within MCSs does not prevent cell stimulation but does require more intense stimulation to activate the complexes, which leads to less controlled stimulation and thus pathology.

Methods

Cells, constructs, antibodies and chemicals: The present studies used HEK (ATCC® CRL-1573™) and HeLa cells (ATCC® Number: CRM-CCL-2) obtained from ATCC. STIM1, Orai1 and SARAF clones have been previously described (Maleth et al., 2014). Ist2 was a kind gift from Dr. James Rothman (Yale University), mCherry-PMCA4 was a kind gift from Dr. Agnes Enyedi (Semmelweis University, Budapest, Hungary) and mCherry-IP_3R3 was a kind gift from Dr. David Yule (Rochester University). The ANO8 clone was obtained from Open Biosystems, cat# 3711771 and ANO8-YFP was obtained from Origene, cat# MG21901. The primers were obtained from Integrated DNA Technologies, Inc (IDT). All point mutations were generated using the QuikChange Lightning site-directed mutagenesis kit from Agilent Technologies. The FKBP12 and FRB constructs are described in (Korzeniowski et al., 2009) and were a kind gift from Dr. Tamas Balla (NIH). PLCδ1 PH-EGFP (Cat #21179) and ER-GECO 1 (Cat # 61244) were purchased from Addgene. In all experiments total cDNA in all transfections was kept the same by supplementing the control condition with appropriate empty vector.
Antibodies used in the present work are: polyclonal anti-GFP (Life Technologies, Cat # A11122) 1:1000 dilution, monoclonal anti-FLAG (Sigma Cat #F3165) 1:1000 dilution; monoclonal anti-MYC (Cell Signaling Inc., Cat # 2276) 1:1000 dilution; anti-HA (Cell Signaling Inc., Cat # 2367S) 1:1000 dilution; anti STIM1 (BD biosciences Cat # 610954) 1:1000 dilution; anti IP3R (BD transduction Laboratories, Cat #610312) 1:1000 dilution; anti-PMCA4a (Santa Cruz, Cat # sc-20028); anti- SERCA (Novus Laboratories, Cat # NB300-581) 1:1000 dilution; Anti-ANO8 (Protein tech Cat # 19485-i-AP) 1:1000 dilution. Carbachol (Sigma, Y0000113), Adenosine 5′-triphosphate magnesium salt (A9187) and Atropine (A0132) were obtained from Sigma-Aldrich. Cyclopiazonic acid (CPA) was from Alomone lab (Cat # C0750).

siRNA probes and qPCR: HEK293 cells were plated at 70–80% confluence and transfected with duplexes after 12 h (100 nM/well) in a 6-well plate. The cells were harvested after 48 h; RNA was extracted using the TRIZOL reagent and the mRNA levels were determined by quantitative PCR. In brief, isolated mRNA was reverse-transcribed into cDNA by the iScript cDNA synthesis kit from Bio-Rad Laboratories. The primers for qPCR for ANO8 and GAPDH were purchased from Applied Biosystems. The fold change in the transcript levels of ANO8 was calculated by normalizing the Ct values from control and siRNA-transfected cells (threshold values) to GAPDH. The plasmids for STIM1 and the mutants were transfected after 48 h of siRNA transfection and the cells were imaged for Ca^{2+} or used for current measurement 24 h after transfection.

$PI(4,5)P_2$ depletion: Depletion of plasma membrane $PI(4,5)P_2$ was accomplished with the FRB/FKBP system as described in (Toth, Toth et al., 2012, Varnai, Thyagarajan et al., 2006). Lyn- FRB localized to the plasma membrane and 5'-phosphatase fused to FKBP12 tagged with mRFP is in the cytosol. The two constructs were co-expressed in the cells. Upon exposure of the cells to 0.2 μM rapamycin for 2 mins, the FRB and the FKBP12 heterodimerize to recruit the phosphatase to the plasma membrane, which hydrolyzes the plasma membrane $PI(4,5)P_2$.

Electrophysiology: HEK293 cells were maintained in Dulbecco's modified Eagle's medium (DMEM) supplemented with 10% fetal bovine serum (FBS) and 1% Pen/Strep. Cells were

transiently transfected using Lipofectamine 2000 (Invitrogen, Carlsbad, CA, USA) with Orai1, STIM1 with or without ANO8 or the ANO8 mutants in a 1:2:2 ratio for 24 h at 37°C. Treatment with siSARAF was with 20-40 nM and with siANO8 was with 100 nM. On the day of experiments, transfected cells were released and plated on square coverslips in 35-mm cell culture dishes and incubated with culture media for at least 2 h to allow attachment to the coverslip. Patch clamp pipettes were pulled from glass capillaries (Warner Instruments) using a vertical puller (PC-10; Narishige) and had a resistance of 5–7 MΩ when filled with the pipette solution. The pipette solution contained (mM) 135 Cs-methanesulfonate, 6 $MgCl_2$, 2 MgATP, 10 HEPES and either 3 EGTA or 10 BAPTA, pH 7.4 (with CsOH). After establishing the whole cell configuration, the cells were kept in Ca^{2+} free solution for 3 min to allow store depletion before exposing the cells to bath solution containing 10 mM Ca^{2+}. The standard bath solution contained (mM) 130 NaCl, 5 KCl, 1 $MgCl_2$, and 10 HEPES with or without 10 $CaCl_2$ (pH 7.4 with NaOH). Whole cell currents were recorded using an Axopatch 200B amplifier (Molecular Devices) with low-pass filtering at 1 kHz. The currents were digitized at a sampling frequency of 5 kHz using Digidata 1440A (Axon Instruments) and stored directly to a hard drive. Current recording was done with PClamp 10 software, and analysis was done with the help of Clampfit software. The current was recorded by 400-ms rapid alterations of membrane potential (RAMP) from -100 to +100 mV from a holding potential of 0 mV. RAMPs were spaced at 4-s intervals. The current recorded at -100 mV was used to calculate current density as pA/pF. For calculating the inactivation slope, the inactivation was fitted with straight line equation y = a + b*x, where b is the slope, a is the value where the line intersects the y-axis. The means of multiple experiments are given as mean ± SEM of the number of experiments performed.

Electron Microscopy: Cells grown on thermonax coverslips were fixed in a mixture of 2.5% paraformaldehyde and 2.0% glutaraldehyde in 0.1 M sodium cacodylate buffer (SCB; pH= 7.4) for 1 hr, followed by extensive wash in SCB. Then samples were postfixed in 2.0% osmium tetroxide plus 1.6% potassium ferricyanide in the above buffer for 60 min. After several rinses in the SCB, the samples were dehydrated in a series of ethanol (30%, 50%, 75%, 95% for 5 min and 100% for 20 min with 3 changes) and infiltrated with Epon-Aradite (Ted Pella, Redding, CA) (50% for 1h and 100% for 1 day with 2 changes). Samples were polymerized at 60 ºC for 30h.
Ultrathin sections (about 80 nm) were cut on Leica EM UC6 Ultramicrotome (Leica, Buffalo Grove, IL) and collected on copper slot grids. Sections were counter-stained with uranyl acetate and lead citrate and examined under a FEI Tecnai12 transmission electron microscope (FEI, Hillsboro, Oregon) operating at beam acceleration voltage of 120keV. Images were acquired by using a Gatan 2k x 2k cooled CCD camera (Gatan, Warrendale, PA).

Co-immunoprecipitation and biotinylation: For co-immunoprecipitation, the cells were harvested in 500 µl of binding buffer (10 mM $NaVO_3$, 10 mM $Na_4P_2O_7$, 50 mM NaF, pH 7.4, and 1% Triton X-100 in PBS), sonicated, and spun down at 13,000 rpm for 5 min. Cell extracts were incubated with the indicated antibodies overnight at 4°C and then incubated with Protein G Sepharose 4 Fast Flow beads (GE Healthcare, Cat #17-0618-01) for 2 h at 4°C. Beads were collected and washed three times with lysis buffer, and proteins were released by heating in 40 µl sample buffer at 56°C for 20 min. Ten µl of each sample was subjected to SDS-PAGE and subsequently transferred to methanol-soaked Nitrocellulose membranes for Western blot analysis.
For biotinylation, cells were incubated with 0.5 mg ml−1 EZ-Sulfo-NHS-LC-biotin (Thermo Scientific, Waltham, MA, USA, Cat #21335) for 30 min on ice, then incubated with 100 mM glycine for 10 min to quench the free biotin and washed with PBS. Lysates were prepared in lysis buffer (contained (mM) 20 Tris, 150 NaCl, 2 EDTA, with 1% Triton X-100, and a protease inhibitor mixture). After sonication, the lysates were centrifuged at 13,000 rpm for 20 min at 4°C, and protein concentration in the supernatants was determined. Biotinylated proteins were isolated with High Capacity NeutrAvidin Agarose beads (Thermo Scientific, Cat #29204) by incubation for 4 h on ice. The beads were washed with lysis buffer and proteins were recovered

by heating with sample buffer at 56°C for 20 min. After separation by SDS-PASE the blots were analyzed for Orai1, STIM1 and ANO8.

Measurement of free cytoplasmic Ca^{2+}: HEK293 cells were plated on 18 mm coverslips. After 24 h of transfection the cells were loaded with Fura-2 by incubation with 5 μM Fura-2/AM (and 0.02% Pluronic acid (Teff labs) for 30-40 min at 37^{o}C in culture media. Coverslips were assembled into a perfusion chamber and the cells continually perfused with warm (37 ^{o}C) media. Fura-2 fluorescence was measured with a TILL photonics Ca^{2+} imaging system at excitation wavelengths of 340 and 380 nm and light emitted at above 500 nm was collected. Collected images were analyzed using MetaFluor and the results are given as the 340/380 ratio. The standard bath solution contained (mM) 140 NaCl, 10 HEPES, 10 Glucose, 5 KCl, 1 $MgCl_2$, and either 1 mM $CaCl_2$ or 0.2 mM EGTA (Ca^{2+}-free). Results are presented as the mean ± SEM from at least three experiments and 30–60 cells/experiment.

Measurement of ER Ca^{2+}: Cells were plated on glass bottom dishes (MatTek Corporation) and transiently transfected with ER-GECO1 and the indicated plasmids. Cells were imaged after 24 h of transfection using 60×, 1.45 NA CFI Apo objective (Nikon) mounted on a Ti-Eclipse inverted microscope with Perfect Focus System (PFS; Nikon). Cells were illuminated with a 559-nm light-emitting diode laser for visualizing ER-LAR-GECO1. Images were collected using a iXon EMCCD Camera (Andor) and NIS elements AR software and analyzed using NIS elements and plotted using Origin 9.4 software (OriginLab). The ER-GECO1 fluorescence was normalization to the initial fluorescence in the presence of ANO8. Since GECO1 is not ratiometric dye, the fluoresce was determined as F/Fo and the initial ratio with ANO8 is taken as 1. All other ratios were determined with respect to the initial ratio in the various experiments and then averaged.

Confocal imaging: HeLa cells were plated on glass bottom dishes and transfected with the indicated construct for 24 h. Cells were washed and incubated with media containing 1 mM Ca^{2+} (control) or media containing 0.2 mM EGTA (Ca^{2+} free) and 25 μM CPA for 7-10 min (store depleted) before imaging. The images were captured at room temperature with a confocal system (FV1000; Olympus) equipped with a UplanSApo 60× oil immersion objective (NA 1.35; Olympus) at 3× zoom. CFP was recorded with 440 nm laser line, YFP was recorded with a 488 nm laser line and mCherry with 568 nm laser line. When more than one color was used, CFP was recorded with 440 nm laser line and YFP with 515 nm laser line and images were recorded sequentially to prevent bleed-through between channels.

TIRF measurements: For TIRF microscopy, HeLa cells were plated on glass bottom dishes and transfected with the indicated constructs. Cells were treated with 25μM CPA in Ca^{2+} free media to initiate STIM1-Orai1 clustering. TIRF microscopy was with a 60×, 1.45 NA CFI Apo objective (Nikon) mounted on a Ti-Eclipse inverted microscope with Perfect Focus System (PFS; Nikon). Images at the TIRF plane were collected using a iXon EMCCD Camera and NIS element AR software. For analysis we defined a punctum as a standalone bright spot formed by a cluster of fluorescently tagged proteins at the TIRF plane. The size and intensity of the puncta were variable. The images from each channel were imported into ImageJ as an image sequence. The brightness threshold was adjusted in ImageJ so that the few puncta present at the beginning of the time course would be included in the data without including the cell background. The threshold was set in the first frame and kept constant for each cell. The area of the cell, which was determined using the NIS-elements software, was accounted for by dividing the number of puncta counted by the area of the cell. The results are shown as mean±s.e.m and are plotted using Origin 9.4 software (Origin Lab).

FRET measurements: HEK293 cells were plated at low confluence on glass bottom dishes (MatTek Corporation) and transfected with ECFP (donor) and EYFP (acceptor) tagged constructs, for 12-16 h using Lipofectamine 2000 (Invitriogen) at 37°C. FRET imaging was performed at 37°C using a confocal system (FV1000; Olympus) equipped with UplanSApo 60X

oil immersion objective (NA 1.35; Olympus) at 1X zoom. Images were acquired at 10s intervals using the simplified two-cube method for sensitized emission (Navarro-Borelly, Somasundaram et al., 2008),(Wlodarczyk, Woehler et al., 2008). To minimize photobleaching low laser power (1-3%) was used.
Image analysis was performed with NIH ImageJ software. Images were corrected for background fluorescence as necessary. FRET was determined on a pixel-by-pixel basis using a two-step FRET efficiency calculation protocol (Zal & Gascoigne, 2004). Briefly, bleed-through components were removed by generating a corrected FRET image (Fc) according to the equation Fc=IDA − dIDD where IDA and IDD are the background-subtracted FRET and ECFP images, respectively. The microscope-specific bleed-through constants a and d were determined by measuring the bleed-through from cells expressing ECFP or EYFP alone. The derived values were d=IDA/IDD= 0.061±0.0064 (n=52 cells) and a=IDA/IAA=0.02±0.0015 (n=46 cells). In the second step the apparent FRET efficiency (Eapp) was calculated using the algorithm Eapp=Fc/(Fc + GIDD) where Eapp is the fraction of ECFP exhibiting FRET and G is a microscope specific constant derived by measuring the increase in ECFP fluorescence following EYFP acceptor photobleaching with the intramolecular CFP–YFP construct YFP-OASF-CFP (Muik et al., 2011), which was estimated to be 0.69±0.12 (n=18 cells).

Statistics: All averages are shown as mean±s.e.m of the number of experiments listed in the Figs. Differences between the groups were analyzed by unpaired t-test or one or two ways ANOVA using Prism. In all cases, $p<0.05$ or better was considered statistically significant.

Acknowledgements

We thank Drs. James Rothman (Yale University), Agnes Enyedi (Semmelweis University, Budapest, Hungary) and David Yule (Rochester University) for providing plasmids for Ist2, mCherry-PMCA4 and mCherry-IP_3R3, respectively. This work was funded by intramural grant from NIH/NIDCR DE000735-07.

Author contributions

AJ, WYC, LV, JM, SL, MA, GZ performed experiments, SM, JA and MA supervised the study and SM drafted the manuscript with contribution from all authors.

Competing interests

All authors declare no conflict of interests.

References

Ahuja M, Jha A, Maleth J, Park S, Muallem S (2014) cAMP and Ca(2)(+) signaling in secretory epithelia: crosstalk and synergism. *Cell Calcium* 55: 385-93
Aoun J, Hayashi M, Sheikh IA, Sarkar P, Saha T, Ghosh P, Bhowmick R, Ghosh D, Chatterjee T, Chakrabarti P, Chakrabarti MK, Hoque KM (2016) Anoctamin 6 Contributes to Cl- Secretion in Accessory Cholera Enterotoxin (Ace)-stimulated Diarrhea: AN ESSENTIAL ROLE FOR PHOSPHATIDYLINOSITOL 4,5-BISPHOSPHATE (PIP2) SIGNALING IN CHOLERA. *J Biol Chem* 291: 26816-26836
Berridge MJ (2016) The Inositol Trisphosphate/Calcium Signaling Pathway in Health and Disease. *Physiol Rev* 96: 1261-96
Besprozvannaya M, Dickson E, Li H, Ginburg KS, Bers DM, Auwerx J, Nunnari J (2018) GRAM domain proteins specialize functionally distinct ER-PM contact sites in human cells. *Elife* 7
Brunner JD, Lim NK, Schenck S, Duerst A, Dutzler R (2014) X-ray structure of a calcium-activated TMEM16 lipid scramblase. *Nature* 516: 207-12

Brzeska H, Guag J, Remmert K, Chacko S, Korn ED (2010) An experimentally based computer search identifies unstructured membrane-binding sites in proteins: application to class I myosins, PAKS, and CARMIL. *J Biol Chem* 285: 5738-47
Chang CL, Hsieh TS, Yang TT, Rothberg KG, Azizoglu DB, Volk E, Liao JC, Liou J (2013) Feedback regulation of receptor-induced Ca2+ signaling mediated by E-Syt1 and Nir2 at endoplasmic reticulum-plasma membrane junctions. *Cell Rep* 5: 813-25
Chung WY, Jha A, Ahuja M, Muallem S (2017) Ca(2+) influx at the ER/PM junctions. *Cell Calcium* 63: 29-32
Dang S, Feng S, Tien J, Peters CJ, Bulkley D, Lolicato M, Zhao J, Zuberbuhler K, Ye W, Qi L, Chen T, Craik CS, Nung Jan Y, Minor DL, Jr., Cheng Y, Yeh Jan L (2017) Cryo-EM structures of the TMEM16A calcium-activated chloride channel. *Nature*
De Jesus-Perez JJ, Cruz-Rangel S, Espino-Saldana AE, Martinez-Torres A, Qu Z, Hartzell HC, Corral-Fernandez NE, Perez-Cornejo P, Arreola J (2018) Phosphatidylinositol 4,5-bisphosphate, cholesterol, and fatty acids modulate the calcium-activated chloride channel TMEM16A (ANO1). *Biochim Biophys Acta* 1863: 299-312
Derler I, Fahrner M, Muik M, Lackner B, Schindl R, Groschner K, Romanin C (2009) A Ca2(+)release-activated Ca2(+) (CRAC) modulatory domain (CMD) within STIM1 mediates fast Ca2(+)-dependent inactivation of ORAI1 channels. *J Biol Chem* 284: 24933-8
Dickson EJ, Jensen JB, Vivas O, Kruse M, Traynor-Kaplan AE, Hille B (2016) Dynamic formation of ER-PM junctions presents a lipid phosphatase to regulate phosphoinositides. *J Cell Biol* 213: 33-48
Giordano F, Saheki Y, Idevall-Hagren O, Colombo SF, Pirruccello M, Milosevic I, Gracheva EO, Bagriantsev SN, Borgese N, De Camilli P (2013) PI(4,5)P(2)-dependent and Ca(2+)-regulated ER-PM interactions mediated by the extended synaptotagmins. *Cell* 153: 1494-509
Henne WM, Liou J, Emr SD (2015) Molecular mechanisms of inter-organelle ER-PM contact sites. *Curr Opin Cell Biol* 35: 123-30
Higley MJ (2014) Localized GABAergic inhibition of dendritic Ca(2+) signalling. *Nat Rev Neurosci* 15: 567-72
Hodeify R, Selvaraj S, Wen J, Arredouani A, Hubrack S, Dib M, Al-Thani SN, McGraw T, Machaca K (2015) A STIM1-dependent 'trafficking trap' mechanism regulates Orai1 plasma membrane residence and Ca(2)(+) influx levels. *J Cell Sci* 128: 3143-54
Hofer AM, Fasolato C, Pozzan T (1998) Capacitative Ca2+ entry is closely linked to the filling state of internal Ca2+ stores: a study using simultaneous measurements of ICRAC and intraluminal [Ca2+]. *J Cell Biol* 140: 325-34
Hong JH, Li Q, Kim MS, Shin DM, Feske S, Birnbaumer L, Cheng KT, Ambudkar IS, Muallem S (2011) Polarized but differential localization and recruitment of STIM1, Orai1 and TRPC channels in secretory cells. *Traffic* 12: 232-45
Huang WC, Xiao S, Huang F, Harfe BD, Jan YN, Jan LY (2012) Calcium-activated chloride channels (CaCCs) regulate action potential and synaptic response in hippocampal neurons. *Neuron* 74: 179-92
Jha A, Ahuja M, Maleth J, Moreno CM, Yuan JP, Kim MS, Muallem S (2013) The STIM1 CTID domain determines access of SARAF to SOAR to regulate Orai1 channel function. *J Cell Biol* 202: 71-9
Jha A, Ahuja M, Patel S, Brailoiu E, Muallem S (2014) Convergent regulation of the lysosomal two-pore channel-2 by Mg(2)(+), NAADP, PI(3,5)P(2) and multiple protein kinases. *EMBO J* 33: 501-11
Kiselyov K, Wang X, Shin DM, Zang W, Muallem S (2006) Calcium signaling complexes in microdomains of polarized secretory cells. *Cell Calcium* 40: 451-9
Korzeniowski MK, Popovic MA, Szentpetery Z, Varnai P, Stojilkovic SS, Balla T (2009) Dependence of STIM1/Orai1-mediated calcium entry on plasma membrane phosphoinositides. *J Biol Chem* 284: 21027-35
Lahiri S, Toulmay A, Prinz WA (2015) Membrane contact sites, gateways for lipid homeostasis. *Curr Opin Cell Biol* 33: 82-87

Lang F, Eylenstein A, Shumilina E (2012) Regulation of Orai1/STIM1 by the kinases SGK1 and AMPK. *Cell Calcium* 52: 347-54
Lee KP, Yuan JP, Zeng W, So I, Worley PF, Muallem S (2009) Molecular determinants of fast Ca2+-dependent inactivation and gating of the Orai channels. *Proc Natl Acad Sci U S A* 106: 14687-92
Li X, Wu G, Yang Y, Fu S, Liu X, Kang H, Yang X, Su XC, Shen Y (2017) Calmodulin dissociates the STIM1-Orai1 complex and STIM1 oligomers. *Nat Commun* 8: 1042
Liou J, Fivaz M, Inoue T, Meyer T (2007) Live-cell imaging reveals sequential oligomerization and local plasma membrane targeting of stromal interaction molecule 1 after Ca2+ store depletion. *Proc Natl Acad Sci U S A* 104: 9301-6
Liou J, Kim ML, Heo WD, Jones JT, Myers JW, Ferrell JE, Jr., Meyer T (2005) STIM is a Ca2+ sensor essential for Ca2+-store-depletion-triggered Ca2+ influx. *Curr Biol* 15: 1235-41
Lytton J, Westlin M, Burk SE, Shull GE, MacLennan DH (1992) Functional comparisons between isoforms of the sarcoplasmic or endoplasmic reticulum family of calcium pumps. *J Biol Chem* 267: 14483-9
Maass K, Fischer MA, Seiler M, Temmerman K, Nickel W, Seedorf M (2009) A signal comprising a basic cluster and an amphipathic alpha-helix interacts with lipids and is required for the transport of Ist2 to the yeast cortical ER. *J Cell Sci* 122: 625-35
Mak DO, Foskett JK (2015) Inositol 1,4,5-trisphosphate receptors in the endoplasmic reticulum: A single-channel point of view. *Cell Calcium* 58: 67-78
Maleth J, Choi S, Muallem S, Ahuja M (2014) Translocation between PI(4,5)P2-poor and PI(4,5)P2-rich microdomains during store depletion determines STIM1 conformation and Orai1 gating. *Nat Commun* 5: 5843
Marchi S, Patergnani S, Missiroli S, Morciano G, Rimessi A, Wieckowski MR, Giorgi C, Pinton P (2017) Mitochondrial and endoplasmic reticulum calcium homeostasis and cell death. *Cell Calcium*
Muallem S, Chung WY, Jha A, Ahuja M (2017) Lipids at membrane contact sites: cell signaling and ion transport. *EMBO Rep* 18: 1893-1904
Muallem S, Pandol SJ, Beeker TG (1989) Hormone-evoked calcium release from intracellular stores is a quantal process. *J Biol Chem* 264: 205-12
Muik M, Fahrner M, Schindl R, Stathopulos P, Frischauf I, Derler I, Plenk P, Lackner B, Groschner K, Ikura M, Romanin C (2011) STIM1 couples to ORAI1 via an intramolecular transition into an extended conformation. *EMBO J* 30: 1678-89
Mullins FM, Park CY, Dolmetsch RE, Lewis RS (2009) STIM1 and calmodulin interact with Orai1 to induce Ca2+-dependent inactivation of CRAC channels. *Proc Natl Acad Sci U S A* 106: 15495-500
Murphy SE, Levine TP (2016) VAP, a Versatile Access Point for the Endoplasmic Reticulum: Review and analysis of FFAT-like motifs in the VAPome. *Biochim Biophys Acta* 1861: 952-961
Navarro-Borelly L, Somasundaram A, Yamashita M, Ren D, Miller RJ, Prakriya M (2008) STIM1-Orai1 interactions and Orai1 conformational changes revealed by live-cell FRET microscopy. *J Physiol* 586: 5383-401
Nunes-Hasler P, Demaurex N (2017) The ER phagosome connection in the era of membrane contact sites. *Biochim Biophys Acta* 1864: 1513-1524
Palty R, Raveh A, Kaminsky I, Meller R, Reuveny E (2012) SARAF inactivates the store operated calcium entry machinery to prevent excess calcium refilling. *Cell* 149: 425-38
Parekh AB (2017) Regulation of CRAC channels by Ca(2+)-dependent inactivation. *Cell Calcium* 63: 20-23
Park MK, Lomax RB, Tepikin AV, Petersen OH (2001) Local uncaging of caged Ca(2+) reveals distribution of Ca(2+)-activated Cl(-) channels in pancreatic acinar cells. *Proc Natl Acad Sci U S A* 98: 10948-53
Paulino C, Kalienkova V, Lam AKM, Neldner Y, Dutzler R (2017) Activation mechanism of the calcium-activated chloride channel TMEM16A revealed by cryo-EM. *Nature*
Petersen OH (2014) Calcium signalling and secretory epithelia. *Cell Calcium* 55: 282-9
Prakriya M, Lewis RS (2015) Store-Operated Calcium Channels. *Physiol Rev* 95: 1383-436

Shin DM, Luo X, Wilkie TM, Miller LJ, Peck AB, Humphreys-Beher MG, Muallem S (2001) Polarized expression of G protein-coupled receptors and an all-or-none discharge of Ca2+ pools at initiation sites of [Ca2+]i waves in polarized exocrine cells. *J Biol Chem* 276: 44146-56
Stathopulos PB, Schindl R, Fahrner M, Zheng L, Gasmi-Seabrook GM, Muik M, Romanin C, Ikura M (2013) STIM1/Orai1 coiled-coil interplay in the regulation of store-operated calcium entry. *Nat Commun* 4: 2963
Stohr H, Heisig JB, Benz PM, Schoberl S, Milenkovic VM, Strauss O, Aartsen WM, Wijnholds J, Weber BH, Schulz HL (2009) TMEM16B, a novel protein with calcium-dependent chloride channel activity, associates with a presynaptic protein complex in photoreceptor terminals. *J Neurosci* 29: 6809-18
Suzuki J, Umeda M, Sims PJ, Nagata S (2010) Calcium-dependent phospholipid scrambling by TMEM16F. *Nature* 468: 834-8
Szasz T, Webb RC (2017) Rho-Mancing to Sensitize Calcium Signaling for Contraction in the Vasculature: Role of Rho Kinase. *Adv Pharmacol* 78: 303-322
Toth DJ, Toth JT, Gulyas G, Balla A, Balla T, Hunyady L, Varnai P (2012) Acute depletion of plasma membrane phosphatidylinositol 4,5-bisphosphate impairs specific steps in endocytosis of the G-protein-coupled receptor. *Journal of cell science* 125: 2185-97
Toulmay A, Prinz WA (2012) A conserved membrane-binding domain targets proteins to organelle contact sites. *J Cell Sci* 125: 49-58
Varnai P, Thyagarajan B, Rohacs T, Balla T (2006) Rapidly inducible changes in phosphatidylinositol 4,5-bisphosphate levels influence multiple regulatory functions of the lipid in intact living cells. *The Journal of cell biology* 175: 377-82
Whitlock JM, Hartzell HC (2017) Anoctamins/TMEM16 Proteins: Chloride Channels Flirting with Lipids and Extracellular Vesicles. *Annu Rev Physiol* 79: 119-143
Wlodarczyk J, Woehler A, Kobe F, Ponimaskin E, Zeug A, Neher E (2008) Analysis of FRET signals in the presence of free donors and acceptors. *Biophys J* 94: 986-1000
Ye W, Han TW, Nassar LM, Zubia M, Jan YN, Jan LY (2018) Phosphatidylinositol-(4, 5)-bisphosphate regulates calcium gating of small-conductance cation channel TMEM16F. *Proc Natl Acad Sci U S A* 115: E1667-E1674
Zal T, Gascoigne NR (2004) Photobleaching-corrected FRET efficiency imaging of live cells. *Biophys J* 86: 3923-39

Fig legends

Fig 1: ANO8 increases interaction of STIM1-Orai1-SARAF and STIM1-STIM1 at the ER/PM junctions

Here and in other experiments, the first number in parenthesis indicates the number of experiments and the second number the number of total cells analyzed. All results are given as mean±s.e.m of the indicated number of experiments or cells analyzed. Panel (**a**): HEK cells transfected with STIM1, Orai1, and with (red) or without ANO8 (black) were used to measure CRAC current with pipette solution (cytoplasmic buffer) containing 3 mM EGTA. Panel (**b**): Same conditions as in (**a**), except that the cells were treated with scrambled (black) or ANO8 siRNA (red). Panel (**c**): Fura2-loaded HEK cells transfected with YFP (control, black) or ANO8 (red) were used to measure store-mediated Ca^{2+} influx. Stores were depleted by treatment with

the SERCA inhibitor CPA and Ca^{2+} influx was measured by Ca^{2+} add-back. Panel (**d**): FRET efficiency was measured with HEK cells transfected with STIM1-CFP, ANO8-YFP, and with (red) and without (black) Orai1-HA before and after store depletion. Here and all other FRET measurements, representative images of the FRET signal under each condition are shown next to the traces. Panel (**e**): FRET efficiency was measured with HEK cells transfected with STIM1-CFP, SARAF-YFP, and with (red) and without (black) untagged ANO8 before and after store depletion. Panel (**f**): Summary of FRET efficiency measurements in panels d-e. Panel (**g**): FRET efficiency was measured with HEK cells transfected with STIM1-CFP, STIM1-YFP (blue), and co-transfected with untagged ANO8 (green) or treated with siANO8 (red) before and after store depletion. Panel (**h**): Resting (R=resting) or store-depleted cells (S=stimulated) HEK cells transfected with STIM1-YFP and myc-STIM1 and with or without ANO8 or treated with siANO8, were used to immunoprecipitate (IP) STIM1-YFP and blot (B) for myc-STIM1. The inputs (In) are with anti-myc, anti-YFP or anti-ANO8. (**i**): FRET ratio was measured with HEK cells transfected with STIM1-CFP, Orai1-YFP (black), and co-transfected with untagged ANO8 (red) before and after store depletion. Panel (**j**): TIRF microscopy was used to measure puncta formation at the TIRF field in cells transfected with STIM1-CFP, ANO8-YFP and Orai1-mCherry before and after store depletion. Panel (**k**): Time course of STIM1 puncta formation in cells transfected with STIM1 and Orai1 alone (black) or together with ANO8. Panel (**l**): Effect of ANO8 on the rate of STIM1-STIM1 clustering. Panel (**m**): Effect of ANO8 on the number of STIM1 puncta. Panel (**n**): Effect of ANO8 on the number of Orai1 puncta.

Fig 2: ANO8 increases native and expressed STIM1-Orai1 complexes and the number and size of ER/PM junctions.

Panel (**a**): HEK cells were used to immunoprecipitate (IP) the native ANO8 (A8) or Orai1 (O1) and blotted (B) for STIM1. Panel (**b**): HEK cells treated with scrambled (siScr) or siANO8 were used to IP the native Orai1 (O1) or STIM1 (S1) and blotted (B) for STIM1, Orai1 or ANO8, as indicated. The columns show the mean±s.e.m of 4 independent experiments. R=resting, S=stimulated. Panel (**c**): Co-IP of mycSTIM1-Orai1-HA, mycSTIM1-ANO8-YFP, and Orai1-HA-ANO8-YFP was measured in transfected HEK cells before (R, resting) and in response to store depletion (S, stimulated). Panel (**d**): shows effect of ANO8-YFP on mycSTIM1 and Orai1-HA surface expression (at the ER/PM junction). Panels (**e-g**): show the mean±s.e.m of surface STIM1 (**e**), Orai1 (**f**) and ANO8 (**g**) in resting (R) and store-depleted cells (S). Panel (**h**): Example EM images recorded from HEK cells transfected with empty vector (left) or ANO8

(right). Red arrows mark ER/PM junctions. Panel (**i**): The size and number of ER/PM junctions in 10 vector-transfected (control) and ANO8-transfected cells.

Fig 3: ANO8 is required for maximal STIM1-Orai1 interaction and increases SARAF-independent current inactivation under potent Ca^{2+} buffering

Panel (**a, b**): knockdown of ANO8 (siA8) reduced CRAC current in cells transfected with Orai1 (Orai1 and STIM1 (S1) and buffered with 3 mM EGTA. Panel (**c**): knockdown of ANO8 reduces the native store-dependent Ca^{2+} influx measured in store depleted cells by Ca^{2+} add-back. Panels (**d, e**): knockdown of ANO8 reduced the number of store-dependent STIM1 puncta at the TIRF plane in cells expressing STIM1 and Orai1. (**d**) shows representative images and (**e**) is the summary of 7 experiments. Panels (**f, g**): current was measured with pipette solution contacting the fast and strong Ca^{2+} buffer 10 mM BAPTA in HEK cells transfected with STIM1, Orai1, and with (red) or without ANO8 (black). (**g**) shows the increase in current density at peak current. Note the prominent current inactivation in the presence of ANO8. Panel (**h**): knockdown of SARAF (red) in wild-type cells had no effect on current inactivation in the presence of 10 mM BAPTA. Panel (**i**): knockdown of SARAF did not prevent the ANO8-dependent inactivation in the presence of 10 mM BAPTA.

Fig 4: Plasma membrane $PI(4,5)P_2$ is required for ANO8 function

Panel (**a, b**): Depletion of plasma membrane $PI(4,5)P_2$ with the FRB/FKBP system prevented the ANO8-mediated increase in STIM1-Orai1 current measured in pipette solutions containing 3 mM EGTA (**a**) or 10 mM BAPTA (**b**). Panels (**c**): HEK cells transfected with ANO8-YFP, STIM1-CFP Orai1-HA and FRB and mCherry-FKBP $PI(4,5)P_2$ depleting construct were treated with 0.2 μM rapamycin (rapa) for 5 min and then with 25 μM CPA for 10 min before fixation and imaging by confocal microscopy. Panels (**d**): Mutating ANO8 R948, R950, R951 in RPRRP, a region that is predicted to include an ANO8 $PI(4,5)P_2$ binding site, prevented increased STIM1-Orai1 current and inactivation. Panel (**e**): Mutating ANO8 R949,950,951 to Q reduced translocation of ANO8.

Fig 5: Inhibiting the SERCA pumps, activation of the IP_3Rs and chelation of ER Ca^{2+} reduced ANO8-dependent current inactivation

Panel (**a**): plot of the slope of inactivation as a function of current density in the presence (red) and absence of ANO8 (black). Increasing current density was obtained by varying external Ca^{2+}

between 2-50 mM. Panels (**b, c**): CRAC current was measured in HEK cells expressing STIM1 and Orai1 and in pipette solution containing 3 mM EGTA (**b**) or 10 mM BAPTA (**c**). SERCA pump was inhibited with 25 µM CPA in the red traces, where indicated and 100 µM IP_3 was included in the pipette solution (green in **c**). Panels (**d, e**): experimental protocol and conditions as in (**b, c**) except that cells were also transfected with ANO8. Panels (**f, g**): HEK cells expressing STIM1, Orai1, and ANO8 were used to measure current in pipette solution containing 10 mM BAPTA and with (red) or without (black) 100 µM IP_3 or 10 mM ER Ca^{2+} chelator TPEN (green). The current density (**f**) and the normalized current (**g**) are shown, illustrating the delay in current inactivation by IP_3 and TPEN.

Fig 6: ANO8 assembles Ca^{2+} signaling complexes at the ER/PM junctions

Panels (**a-d**): ER Ca^{2+} content was measured with ER-GECO1 in the periphery (**a**) and the center (**b**) or cells transfected with M3 receptors and with (red, green) or without (black, blue) ANO8. Receptor mediated store depletion was initiated by stimulating the cells with 0.5 mM carbachol in Ca^{2+}-free solution. Cell stimulation was terminated with 10 µM atropine and ER Ca^{2+} uptake was initiated by perfusing the cells with a solution containing 5 mM Ca^{2+}. The fluorescence was measured as F/F_0 and normalized to the initial fluorescence in the presence of ANO8. Panel (**c**) shows traces of ER Ca^{2+} uptake at expanded time scale and the averaged slopes of ER Ca^{2+} influx and (**d**) shows the averaged slope of Ca^{2+} release at the cell periphery (Peri) and cell center (Center). In (**c**) the traces were aligned along the Y axis to better show the difference in uptake rate. Panel (**e**): shows the effect of ANO8 expression of the Co-IP of the native SERCA2 and STIM1 in resting and store depleted cells. The columns are the mean±s.e.m of 3 experiments. Panel (**f**): shows the enhancement by ANO8 of the Co-IP of expressed STIM1 with PMCA4a and SERCA2 and of Orai1 with SERCA2 in resting and store depleted cells. Panel (**g**): shows the FRET ratio between STIM1 and SERCA2 in response to store depletion and its enhancement by ANO8. Panels (**h, i**): Simultaneous measurements of ER Ca^{2+} with ER-GECO1 and $PI(4,5)P_2$ hydrolysis with $PH_{PLC\delta}$-GFP in response to cell stimulation of M3 receptors. Traces are shown in (**h**) and the average slopes are in (**i**). Panel (**j**): shows the effect of ANO8 on the Co-IP of the native STIM1 and IP_3Rs. The columns are the mean±s.e.m of 3 experiments. Panel (**k**): shows the FRET ratio between expressed STIM1 and IP_3R3 in response to store depletion and its enhancement by ANO8. Panel (**l**): shows the FRET ratio between expressed STIM1 and PMCA4 in response to store depletion and its enhancement by ANO8.

Fig 7: ANO8 tunes receptor-evoked Ca^{2+} signaling

Panels (**a-d**): HeLa cells transfected with GFP (black) or ANO8 (red) were stimulated with 0.5 and then 1 μM ATP to activate the native P2Y2 receptors. The oscillations were analyzed in terms of the % of responding cells (**b**), oscillation frequency (**c**), and the amplitude of the Ca^{2+} signal (**d**). Panels (**e-h**): HeLa cells were treated with scrambled siRNA (black) or siANO8 (red) and were stimulated with 1 and then 5 μM ATP. The oscillations were analyzed in terms of the % of responding cells (**f**), oscillations frequency (**g**), and the amplitude of the Ca^{2+} signal (**h**).

Figure 1, Jha et al.

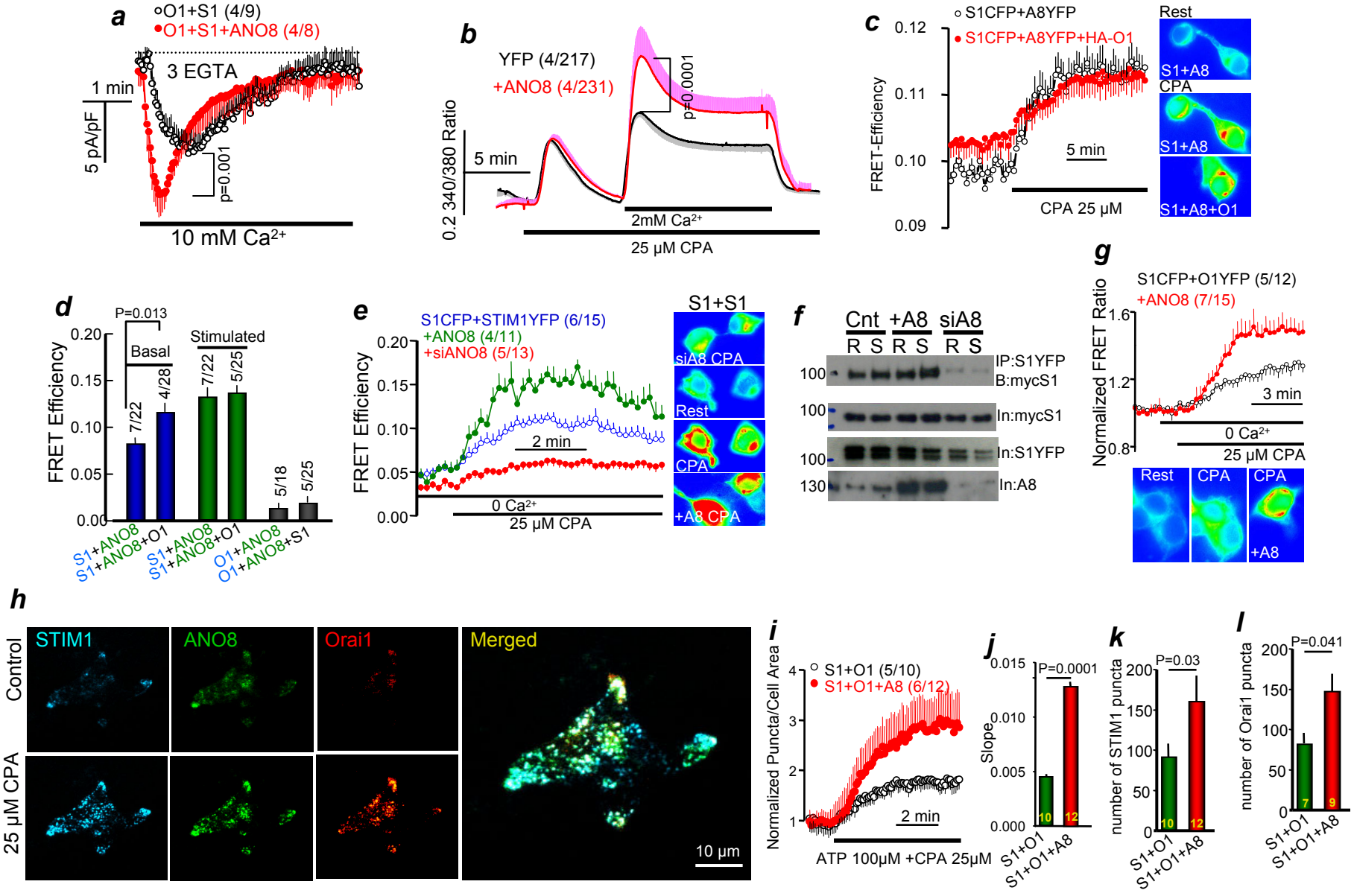

Figure 2, Jha et al.

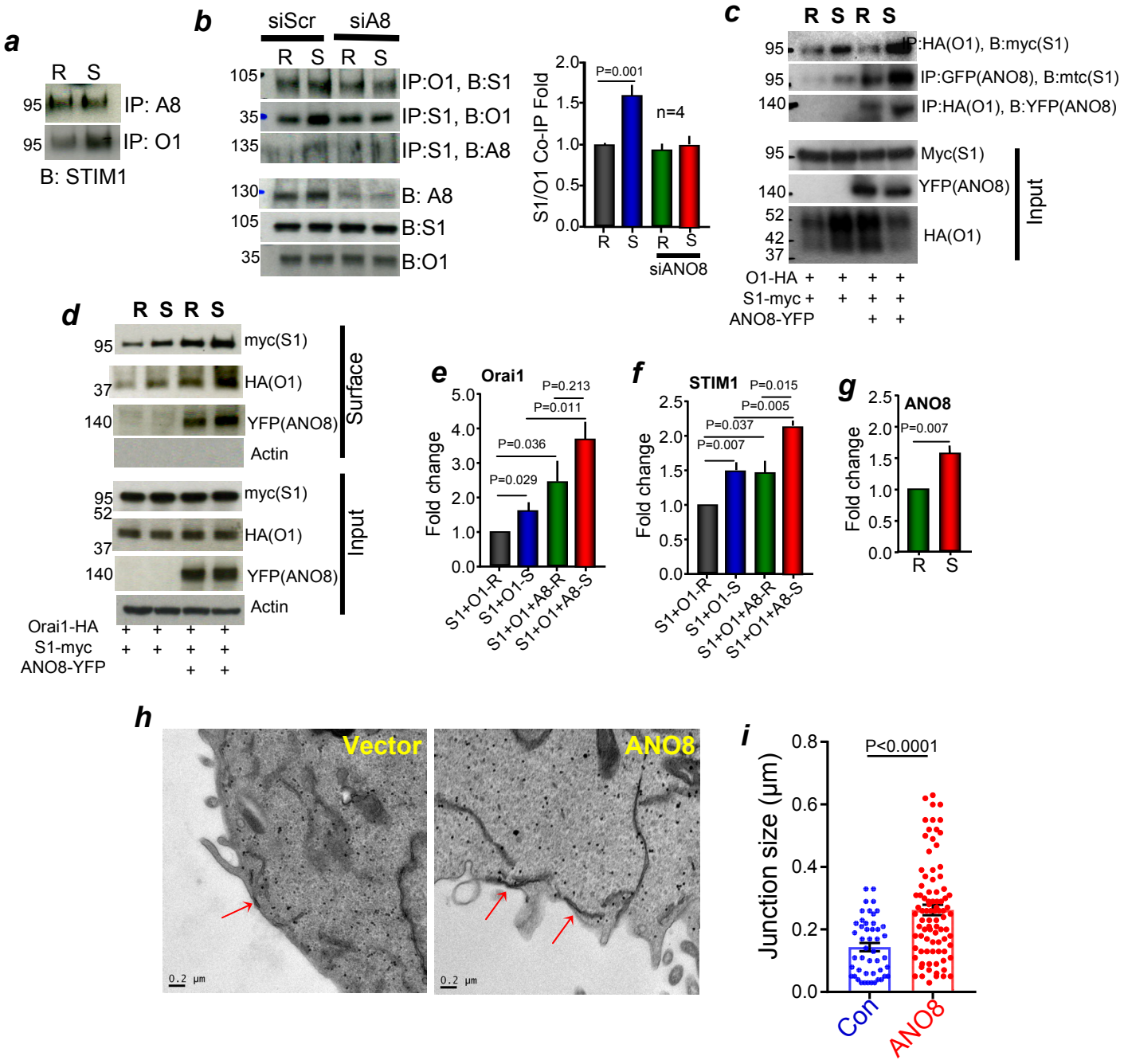

Figure 3, Jha et al.

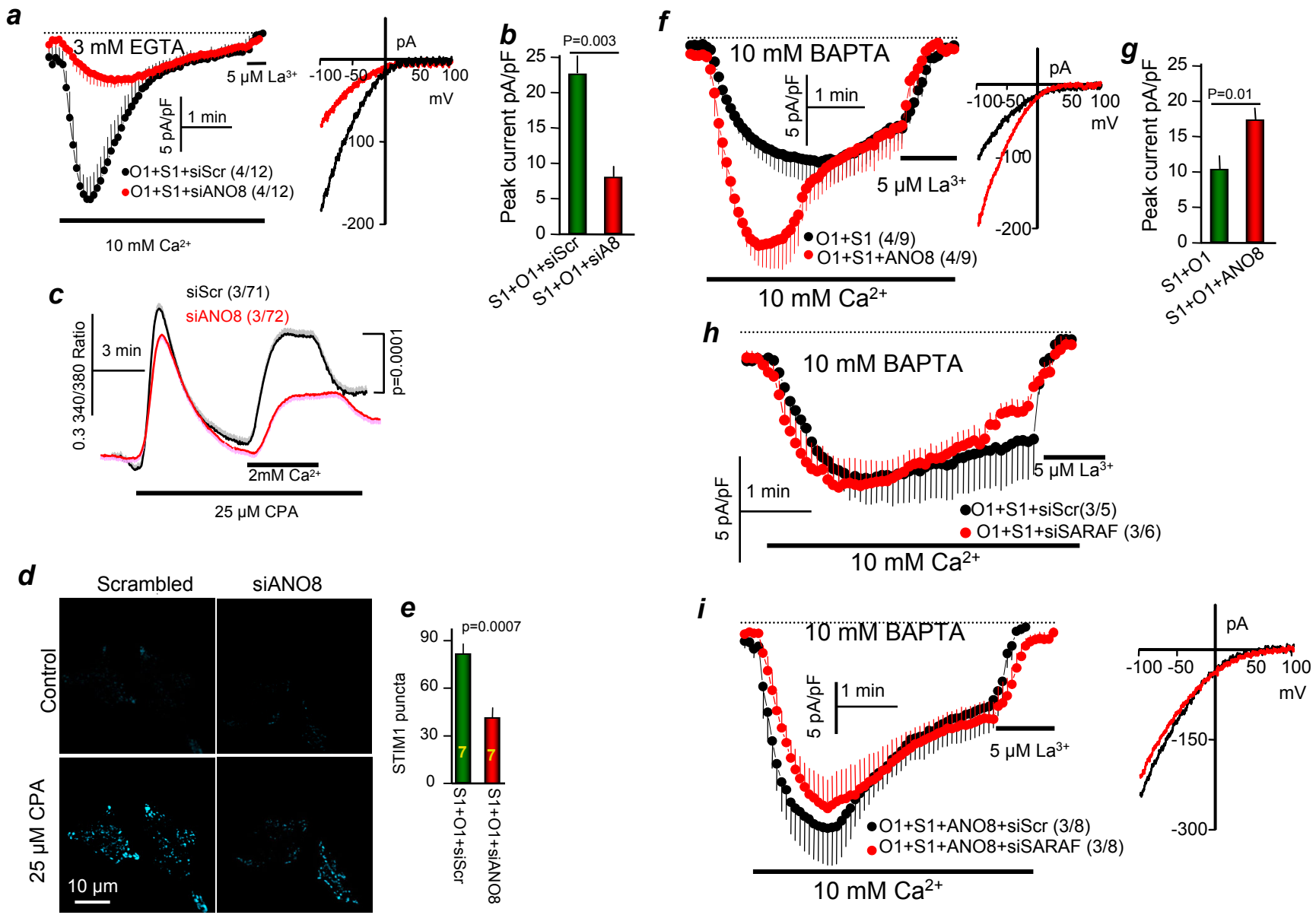

Figure 4, Jha et al.

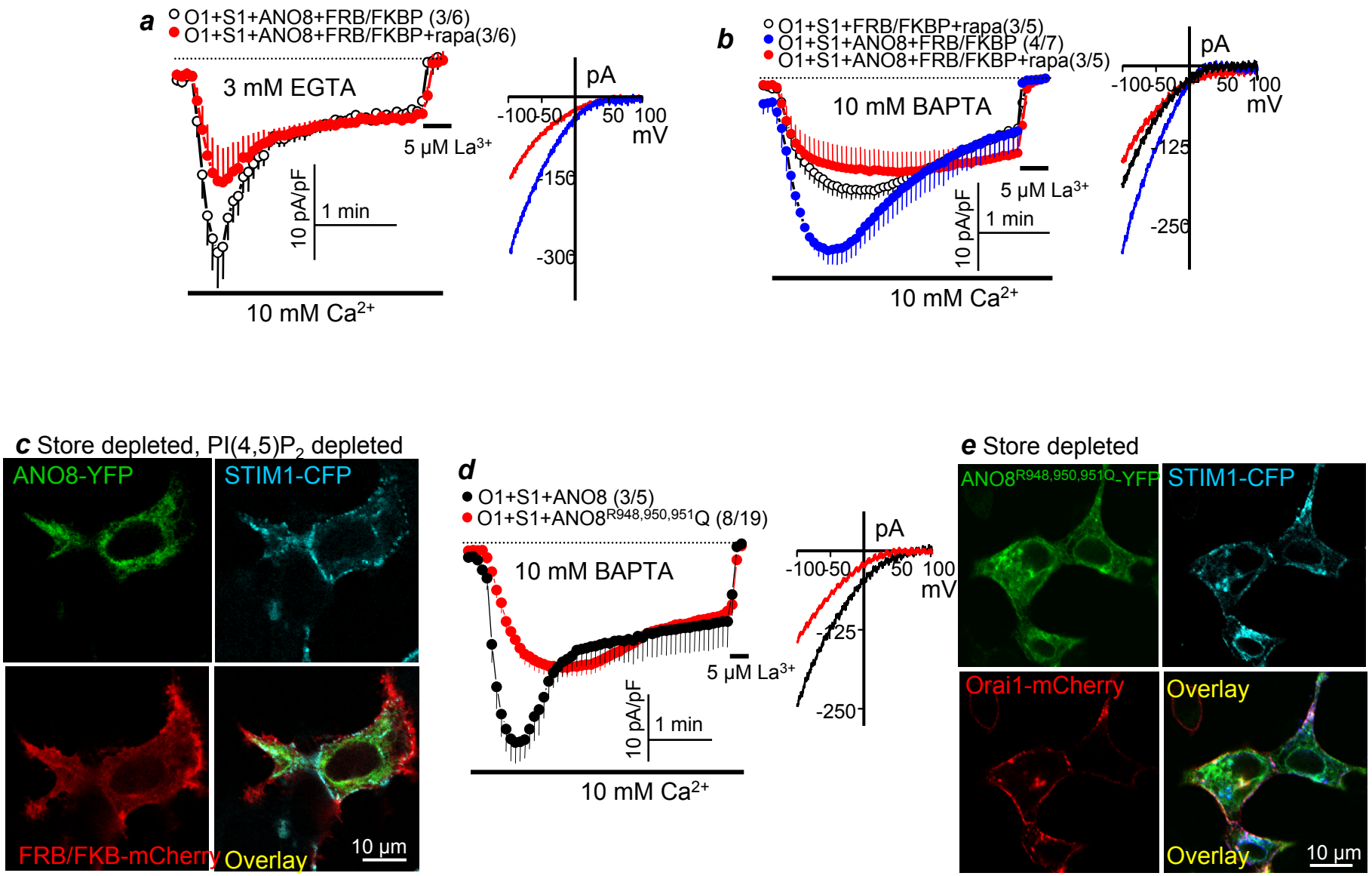

Figure 5, Jha et al.

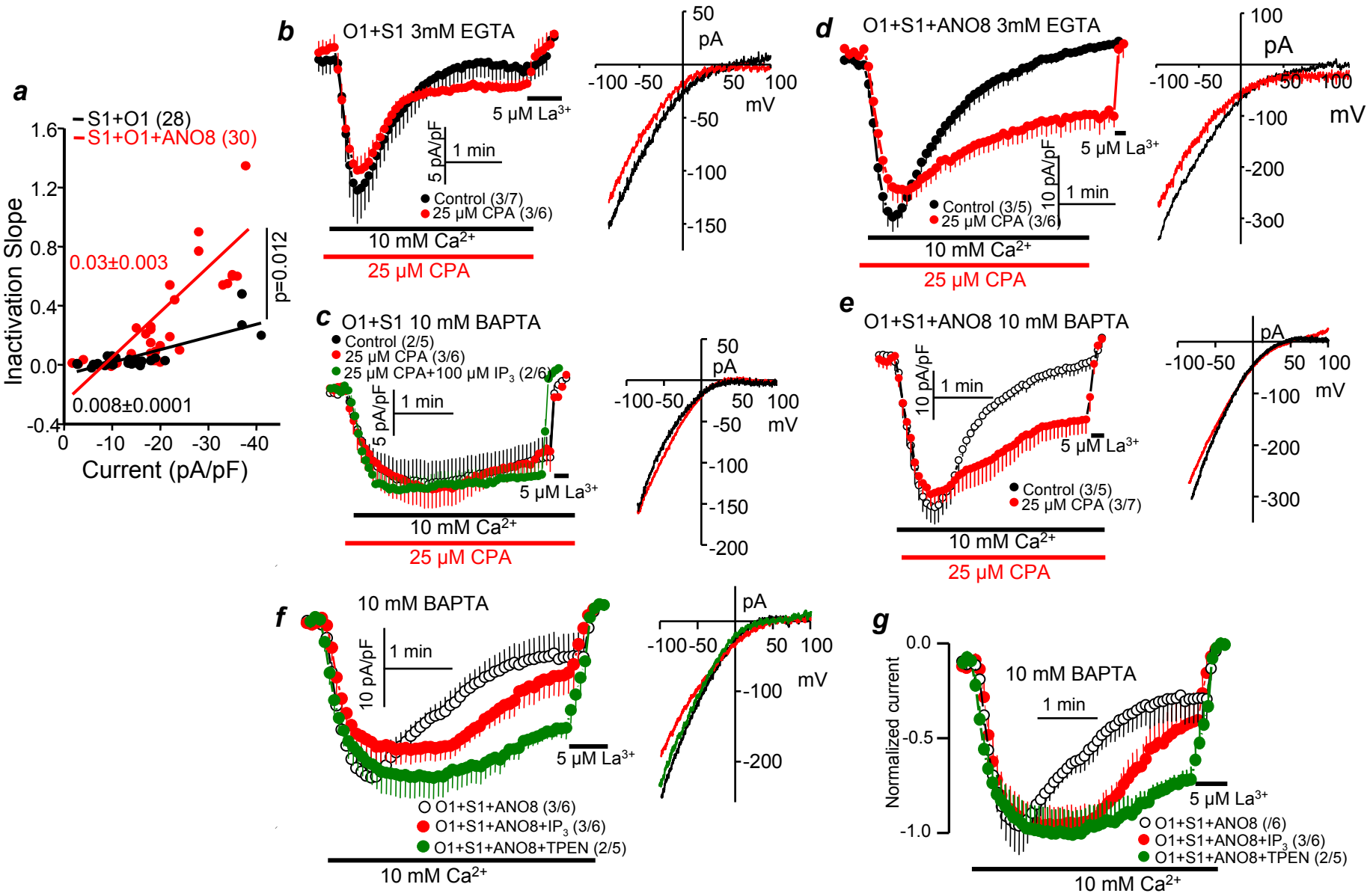

Figure 6, Jha et al.

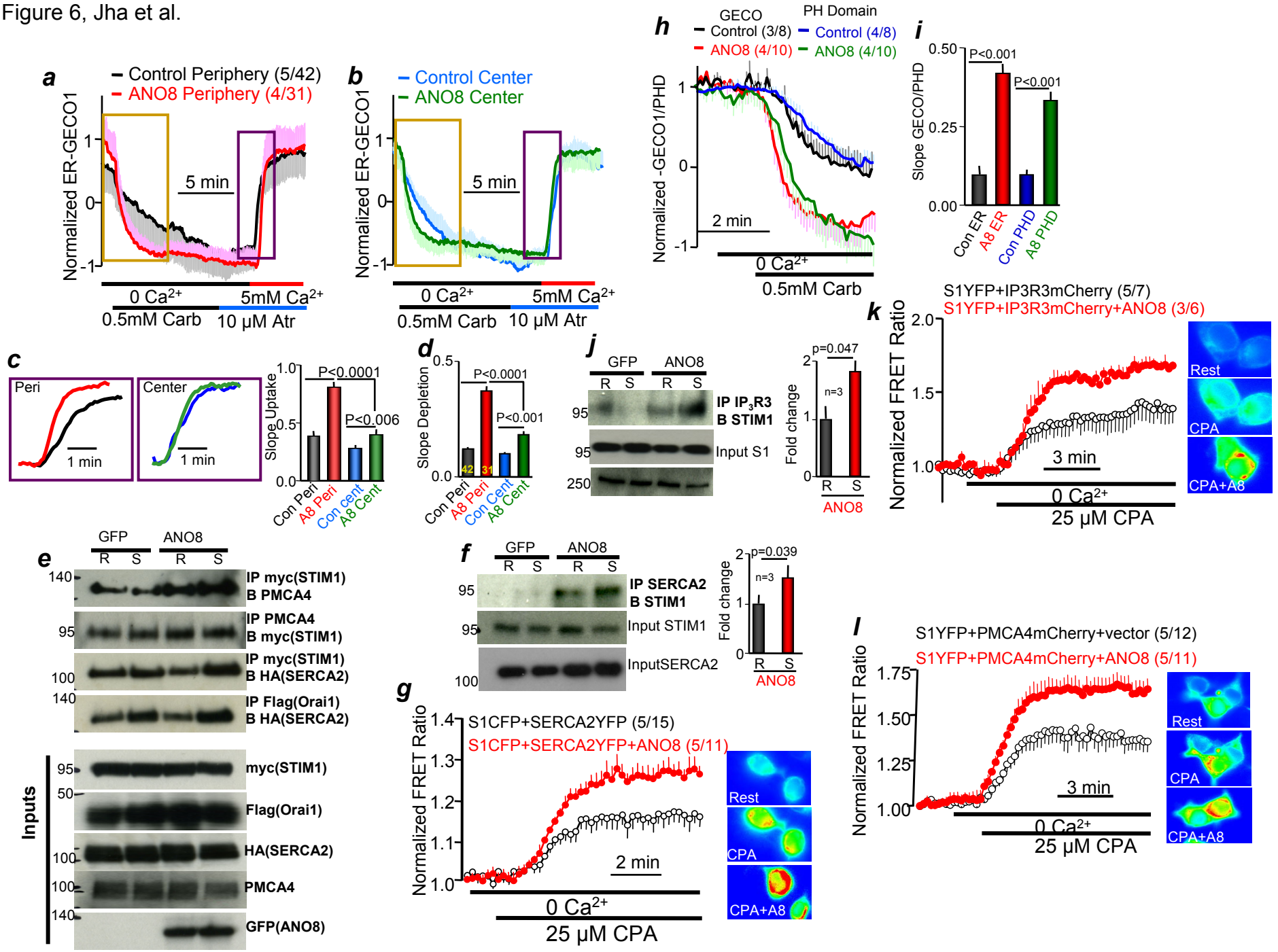

Figure 7, Jha et al.

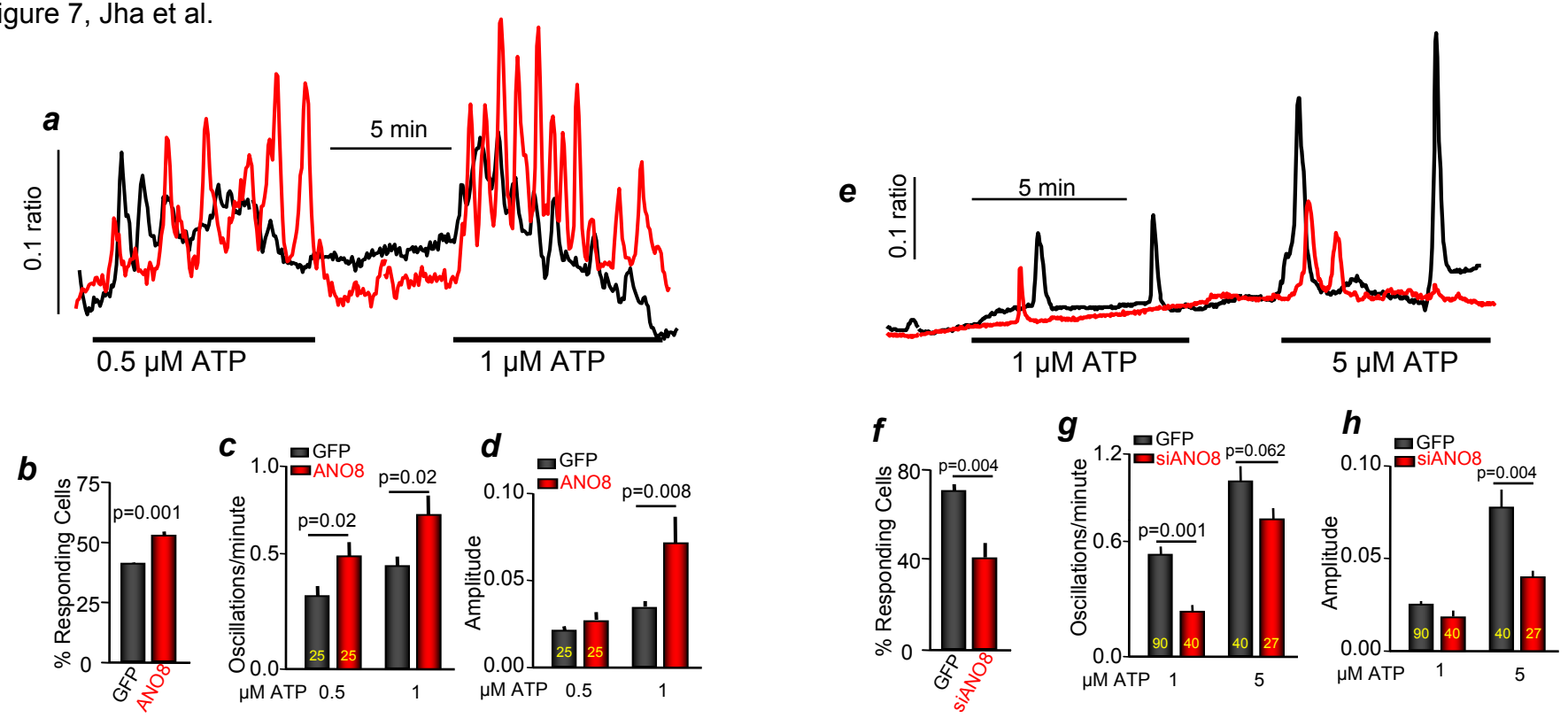

Anoctamin 8 Tether the Endoplasmic Reticulum and Plasma Membranes to Assemble Ca^{2+} Signaling Complexes at the ER/PM Junctions

Archana Jha[1,4], Woo Young Chung[1,4], Laura Vachel[1], Jozsef Maleth[2], Sarah Lake[1], Guofeng Zhang[3], Malini Ahuja[1] and Shmuel Muallem[1,5]

From [1]The Epithelial Signaling and Transport Section, National Institute of Dental and Craniofacial Research, National Institutes of Health, Bethesda, MD 20892, [2]First Department of Medicine, University of Szeged, Szeged, Hungary, [3]Trans-NIH Shared Resource on Biomedical Engineering and Physical Science (BEPS) National Institute of Biomedical Imaging & Bioengineering.

Extended View Information

Methods

Constructs, antibodies and chemicals: STIM1, Orai1 and SARAF clones have been previously described(Maleth, Choi et al., 2014). Ist2 was a kind gift from Dr. James Rothman (Yale university), mCherry-PMCA4 was a kind gift from Dr. Agnes Enyedi (Semmelweis University, Budapest, Hungary) and mCherry-IP_3R3 was a kind gift from Dr. David Yule (Rochester University). The ANO8 clone was obtained from Open Biosystems, cat# 3711771 and ANO8-YFP was obtained from Origene, cat# MG21901. The primers were obtained from Integrated DNA Technologies, Inc (IDT). All point mutations were generated using the QuikChange Lightning site-directed mutagenesis kit from Agilent Technologies. The FKBP12 and FRB constructs are described in(Korzeniowski, Popovic et al., 2009) and were a kind gift from Dr. Tamas Balla (NIH). PLCδ1 PH-EGFP (Cat #21179) and ER-GECO 1 (Cat # 61244) were purchased from Addgene. In all experiments total cDNA in all transfections was kept the same by supplementing the control condition with appropriate empty vector.

Antibodies used in the present work are: polyclonal anti-GFP (Life Technologies, Cat # A11122) 1:1000 dilution, monoclonal anti-FLAG (Sigma Cat #F3165) 1:1000 dilution; monoclonal anti-MYC (Cell Signaling Inc., Cat # 2276) 1:1000 dilution; anti-HA (Cell Signaling Inc., Cat # 2367S) 1:1000 dilution; anti STIM1 (BD biosciences Cat # 610954) 1:1000 dilution; anti-Orai1 (Thermofisher scientific, Cat # PA1-74181) 1:1000 dilution; anti IP3R (BD transduction Laboratories, Cat #610312) 1:1000 dilution; anti-PMCA4a (Santa Cruz, Cat # sc-20028); anti- SERCA (Novus Laboratories, Cat # NB300-581) 1:1000 dilution; Anti-ANO8 (Protein tech Cat # 19485-i-AP) 1:1000 dilution. Carbachol (Sigma, Y0000113), Adenosine 5′-triphosphate magnesium salt (A9187) and Atropine (A0132) were obtained from Sigma-Aldrich. Cyclopiazonic acid (CPA) was from Alomone lab (Cat # C0750).

siRNA probes and qPCR: HEK293 cells were plated at 70–80% confluence and transfected with duplexes after 12 h (100 nM/well) in a 6-well plate. The cells were harvested after 48 h; RNA was extracted using the TRIZOL reagent and the mRNA levels were determined by quantitative PCR. In brief, isolated mRNA was reverse-transcribed into cDNA by the iscript cDNA synthesis kit from Bio-Rad Laboratories. The primers for qPCR for ANO8 and GAPDH were purchased from Applied Biosystems. The fold change in the transcript levels of ANO8 was calculated by normalizing the Ct values from control and siRNA-transfected cells (threshold values) to GAPDH. The plasmids

for STIM1 and the mutants were transfected after 48 h of siRNA transfection and the cells were imaged for Ca^{2+} or used for current measurement 24 h after transfection.

Co-immunoprecipitation and biotinylation: For co-immunoprecipitation, the cells were harvested in 500 µl of binding buffer (10 mM $NaVO_3$, 10 mM $Na_4P_2O_7$, 50 mM NaF, pH 7.4, and 1% Triton X-100 in PBS), sonicated, and spun down at 13,000 rpm for 5 min. Cell extracts were incubated with the indicated antibodies overnight at 4°C and then incubated with Protein G Sepharose 4 Fast Flow beads (GE Healthcare, Cat #17-0618-01) for 2 h at 4°C. Beads were collected and washed three times with lysis buffer, and proteins were released by heating in 40 µl sample buffer at 56°C for 20 min. Ten µl of each sample was subjected to SDS-PAGE and subsequently transferred to methanol-soaked Nitrocellulose membranes for Western blot analysis.

For biotinylation, cells were incubated with 0.5 mg ml−1 EZ-Sulfo-NHS-LC-biotin (Thermo Scientific, Waltham, MA, USA, Cat #21335) for 30 min on ice, then incubated with 100 mM glycine for 10 min to quench the free biotin and washed with PBS. Lysates were prepared in lysis buffer (contained (mM) 20 Tris, 150 NaCl, 2 EDTA, with 1% Triton X-100, and a protease inhibitor mixture). After sonication, the lysates were centrifuged at 13,000 rpm for 20 min at 4°C, and protein concentration in the supernatants was determined. Biotinylated proteins were isolated with High Capacity NeutrAvidin Agarose beads (Thermo Scientific, Cat #29204) by incubation for 4 h on ice. The beads were washed with lysis buffer and proteins were recovered by heating with sample buffer at 56°C for 20 min. After separation by SDS-PASE the blots were analyzed for Orai1, STIM1 and ANO8.

Confocal imaging: HeLa cells were plated on glass bottom dishes and transfected with the indicated construct for 24 h. Cells were washed and incubated with media containing 1 mM Ca^{2+} (control) or media containing 0.2 mM EGTA (Ca^{2+} free) and 25 µM CPA for 7-10 min (store depleted) before imaging. The images were captured at room temperature with a confocal system (FV1000; Olympus) equipped with a UplanSApo 60× oil immersion objective (NA 1.35; Olympus) at 3× zoom. CFP was recorded with 440 nm laser line, YFP was recorded with a 488 nm laser line and mCherry with 568 nm laser line. When more than one color was used, CFP was recorded with 440 nm laser line and YFP with 515 nm laser line and images were recorded sequentially to prevent bleed-through between channels.

Extended View Figure legends

Figure EV1: Effect of knockdown of ANO proteins or ANO proteins on STIM1-Orai1 current

Panels (**a-e**): CRAC current was measured in HEK cells transfected with STIM1-CFP and Orai1-mCherry and treated with scrambled (all black traces) or siRNA to knockout ANO1 (**a**), ANO2 (**b**), ANO3 (**c**), ANO5 (**d**) or ANO9 (**e**). Panels (**f-i**): CRAC current was measured in HEK cells transfected with STIM1-CFP and Orai1-mCherry and empty vector (EV, all black traces) or ANO4 (**f**), ANO6 (**g**), ANO7 (**h**) or ANO10 (**i**).

Figure EV2: Ist2 increases Orai1 current density and SCDI

CRAC current was measured in HEK cells transfected with STIM1-CFP, Orai1-mCherry, and with (red) or without (black) Ist2 and with pipette solution containing 3 mM EGTA.

Figure EV3: ANO8 does not interact with or activate Orai1

Panel (**a**): FRET efficiency was measured with HEK cells transfected with Orai1-mCherry, ANO8-YFP, and with (red) and without (black) myc-STIM1 before and after store depletion. Panel (**b**): Effect of ANO8 on Orai1 current was measured using the STIM1-independent constitutively active mutant Orai1(V102C) transfected alone in control cells (black), together with ANO8 (blue) or in cells treated with siANO8 (red).

Figure EV4: Localization of ANO8 in store replete and depleted cells

Panel (**a**): ANO8 is localized mostly in the ER together with STIM1 in store replete cells. Panel (**b**): ANO8 accumulates in the ER/PM junctions in response to store depletion.

Figure EV5: Knockdown of ANO8 reduces clustering of constitutively active STIM1 mutants at the ER/PM junctions and activation of Orai1.

Panels (**a-c**): HEK cells treated with scrambled (**a**) or ANO8 (**b**) siRNA were transfected with the constitutively active STIM1(D76A). The average number of puncta at the TIRF plane was analyzed in 3 separate experiments with the total number of cells indicated (**c**). Panels (**d, e**): Orai1 current was measured in cells transfected with Orai1 and the constitutively active STIM1-Kras with pipette solution containing 3 mM EGTA and treated with scrambled (black, green) or ANO8 (red) siRNA; (**d**) shows current density and (**e**) is the normalized current, which better demonstrates the effect of ANO8 knockdown on the rate of SCDI. Current started by addition of 10 mM Ca^{2+} to the media. Panel (**f, g**): Orai1 current was measured in cells transfected with Orai1 and the constitutively active STIM1(ΔCTID) with pipette solution containing 10 mM BAPTA. The cells were treated with scrambled (black) or ANO8 (red) siRNA. Current measurement started on establishing the whole cell configuration in media already containing 10 mM Ca^{2+}.

Figure EV6: SARAF modulates Orai1 SCDI and ANO8 increases STIM1-SARAF interaction

Panel (**a**): HEK cells transfected with STIM1-CFP, Orai1-mCherry and treated with scrambled (black) or SARAF siRNA (red) were used to measure CRAC current with pipette solution containing 3 mM EGTA. Panel (**b**): FRET efficiency was measured with HEK cells transfected with STIM1-CFP, SARAF-YFP, and with (red) and without (black) untagged ANO8 before and after store depletion.

Figure EV7: The effects of ANO8 are independent of its Ca^{2+} binding site

Panel (**a**): shows the Ca^{2+} binding sites of the TMEM16 family member from the fungus *Nectria haematococca*(Brunner, Lim et al., 2014) and the corresponding residues of ANO8 (red). Panel

(**b, c**): The ANO1(E734Q) and ANO1(E654Q) mutations shifted the ANO1 Km for Ca^{2+} from 0.36 to 4 μM (**b**) and to more than 2 mM (**c**), respectively (green). The equivalent ANO8(E774Q) (**b**) and ANO8(E485Q) (**c**) mutations had no effect on increased STIM1-Orai1 current density and inactivation measured with pipette solution containing 10 mM BAPTA.

Figure EV8: ANO8 markedly increases current activated by STIM1(ΔK) that is $PI(4,5)P_2$-dependent

Panel (**a**): Current density recorded with pipette solution containing 10 mM BAPTA in cells transfected with STIM1(ΔK), Orai1 and with (red) or without (black) ANO8. Panel (**b, c**): STIM1(ΔK) puncta were recorded with TIRF microscopy of cells expressing STIM1(ΔK), Orai1, and with or without ANO8. Example images are shown in (**b**) and the average of the indicated number of cells in (**c**). Panel (**d**): HEK cells expressing STIM1(ΔK), Orai1, ANO8, FRB, and FKB were used to measure CRAC current without (black) and with treatment with 0.2 μM rapamycin to deplete $PI(4,5)P_2$ (red).

Figure EV9: Predicted potential lipid binding site on ANO8

The sites predicted to bind phospholipids with the highest score are shown in red and the other potential sites are shown in green. The first transmembrane domain (starting with I245) and last residue of the last transmembrane domain (D861) are shown in blue.

Figure EV10: Effect of ANO8 on fast Ca^{2+}-dependent inactivation

Panel (**a**): Shown are current traces from HEK cells transfected with STIM1, Orai1 and with (red) and without (black) ANO8 with pipette solution containing 10 mM BAPTA. Panel (**b**) shows the reduction in current at 400 msec. Panel (**c**): The current traces were fit to two exponentials and the left and right columns show the effect of ANO8 on the first and second exponentials, respectively.

Table EV1: The siRNA primers used and % knockdown of the indicated mRNA

Table EV2: The primers used to generate the indicated mutants in ANO8

References

Brunner JD, Lim NK, Schenck S, Duerst A, Dutzler R (2014) X-ray structure of a calcium-activated TMEM16 lipid scramblase. *Nature* 516: 207-12

Korzeniowski MK, Popovic MA, Szentpetery Z, Varnai P, Stojilkovic SS, Balla T (2009) Dependence of STIM1/Orai1-mediated calcium entry on plasma membrane phosphoinositides. *J Biol Chem* 284: 21027-35

Maleth J, Choi S, Muallem S, Ahuja M (2014) Translocation between PI(4,5)P2-poor and PI(4,5)P2-rich microdomains during store depletion determines STIM1 conformation and Orai1 gating. *Nat Commun* 5: 5843

Figure EV1, Jha et al.

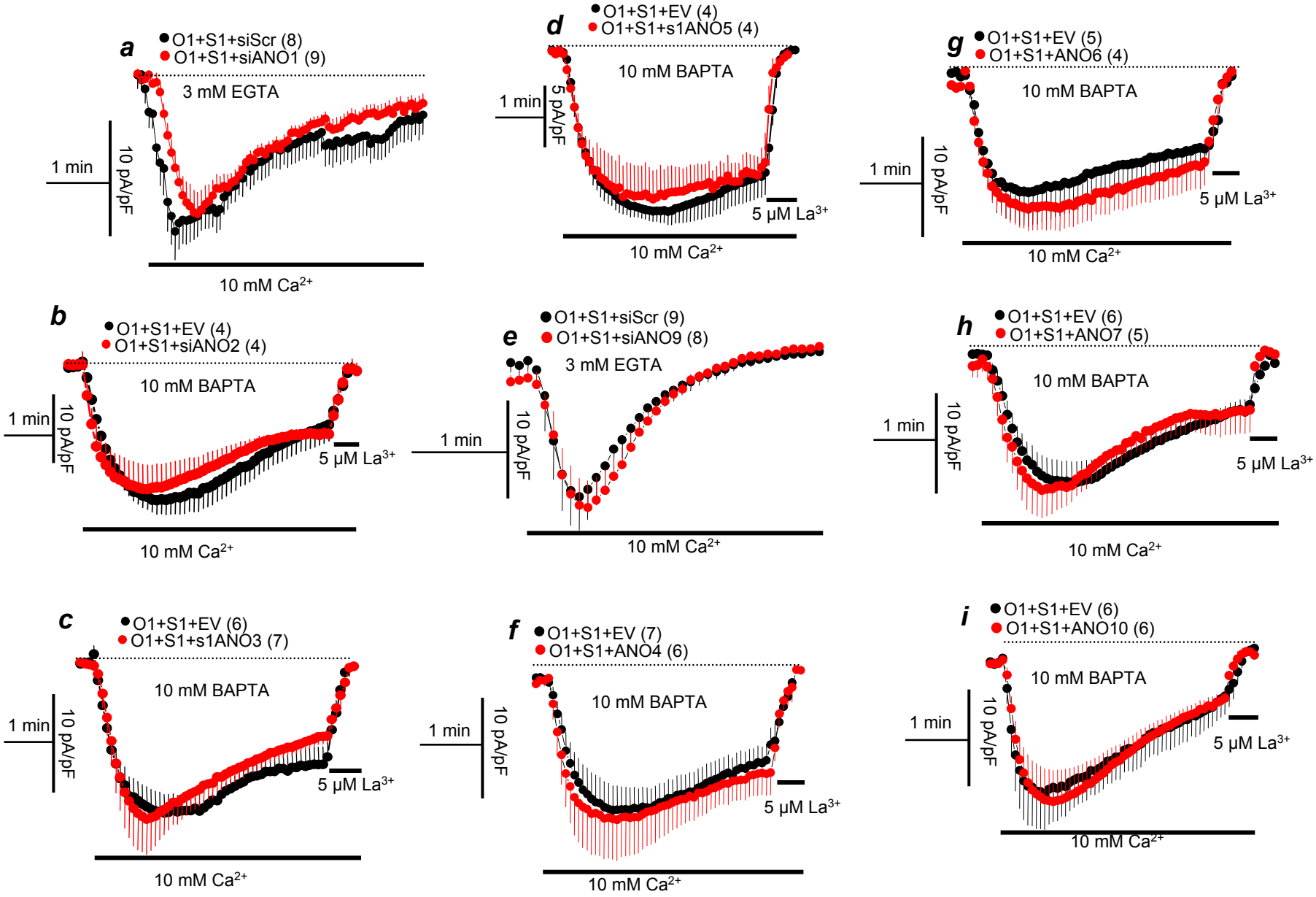

Figure EV2, Jha et al.

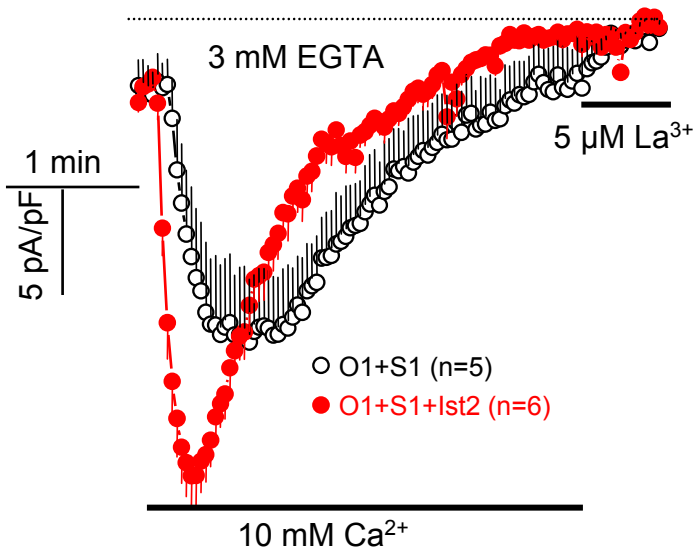

Figure EV3, Jha et al.

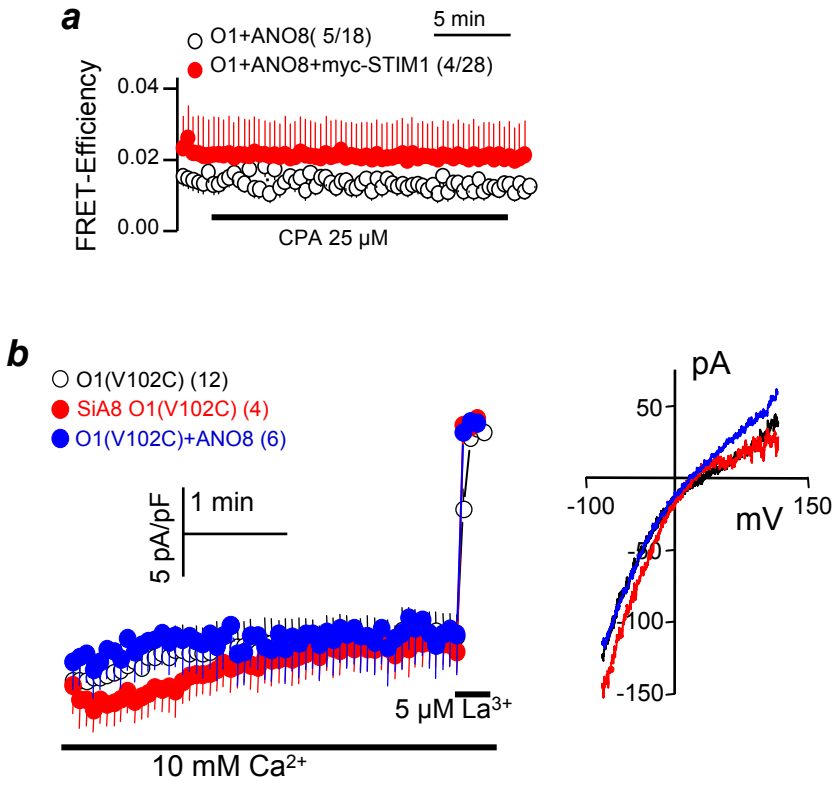

Figure EV4, Jha et al.

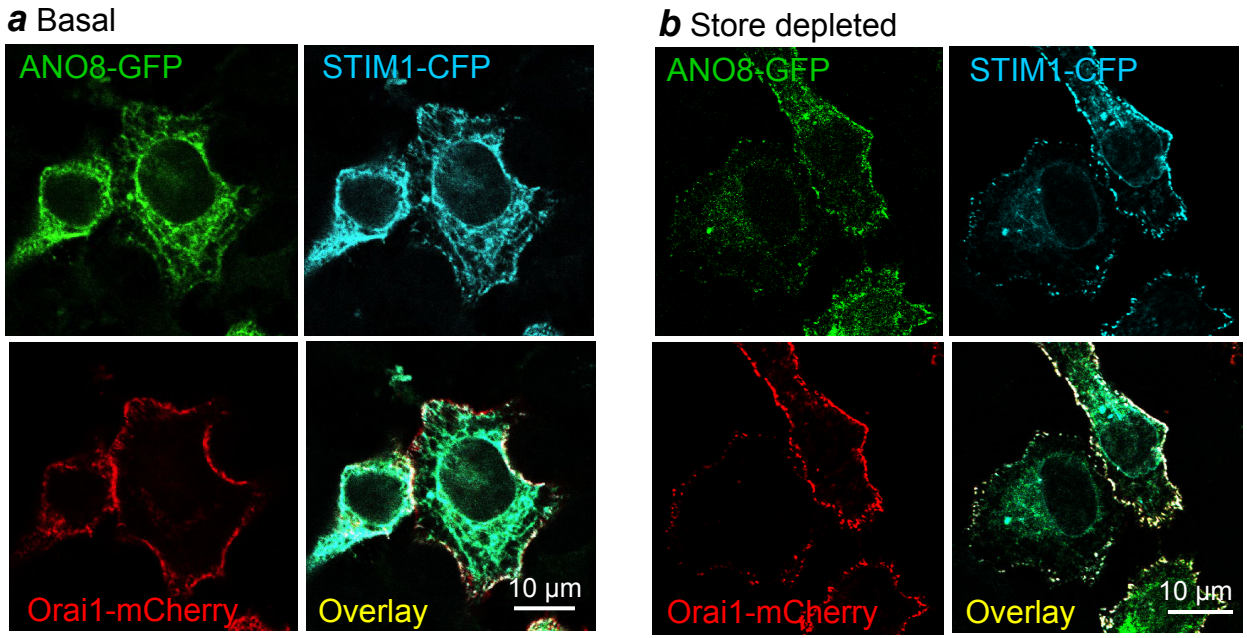

Figure EV5, Jha et al.

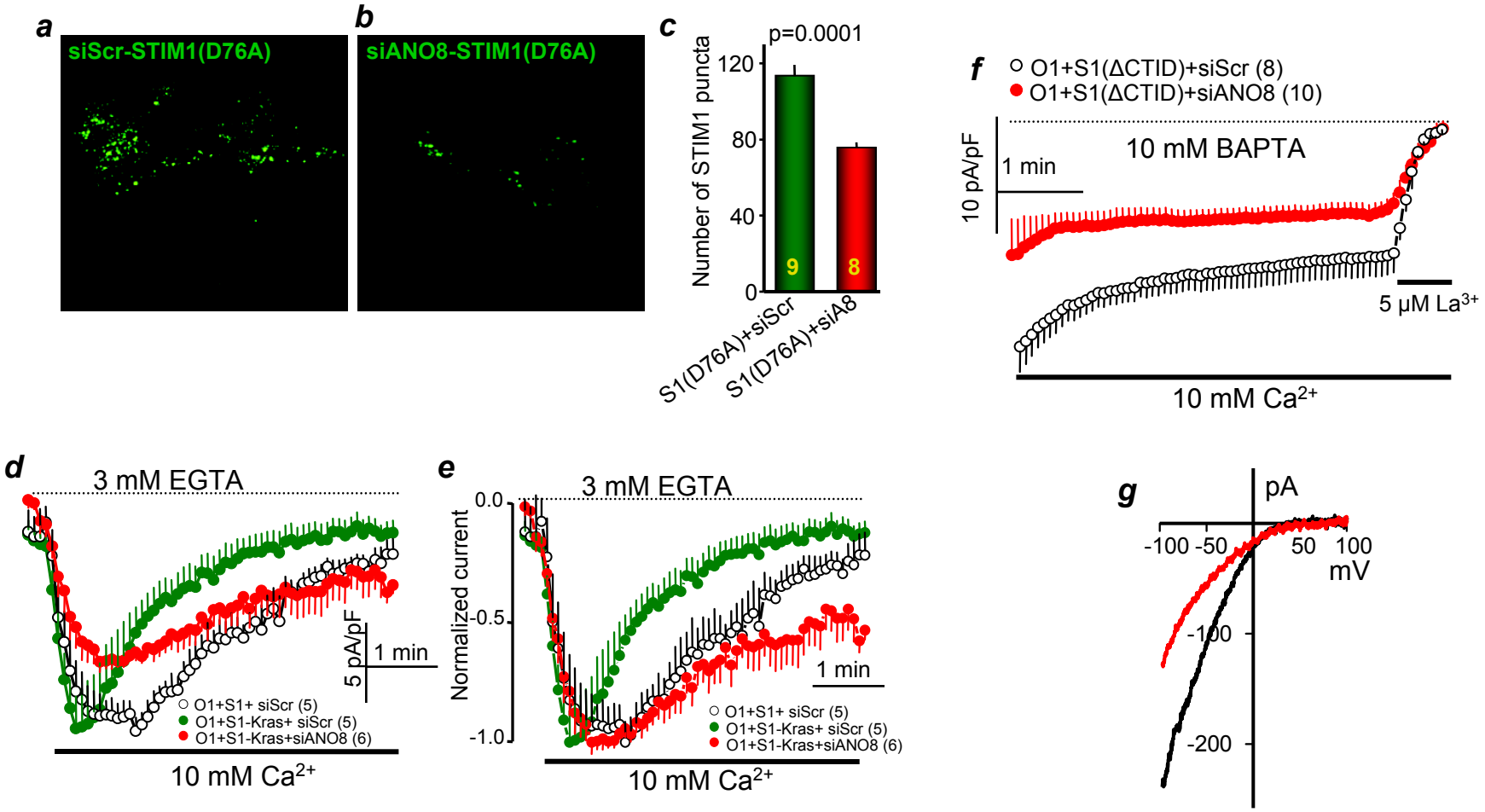

Figure EV6, Jha et al.

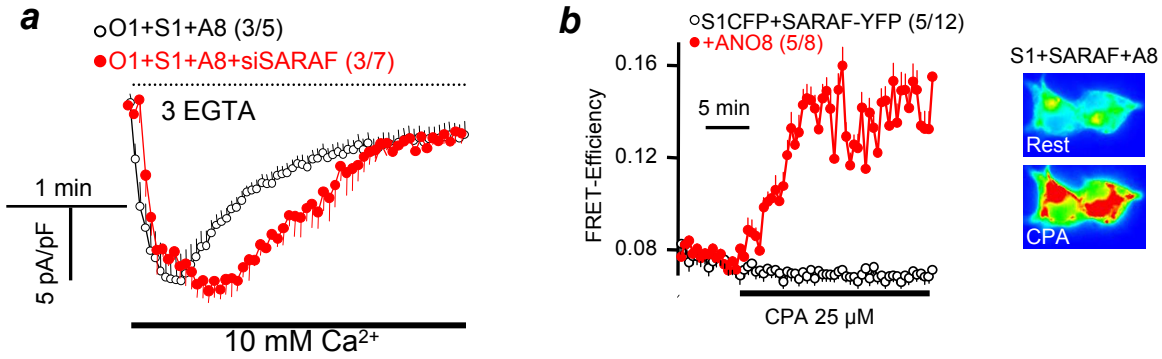

Figure EV7, Jha et al.

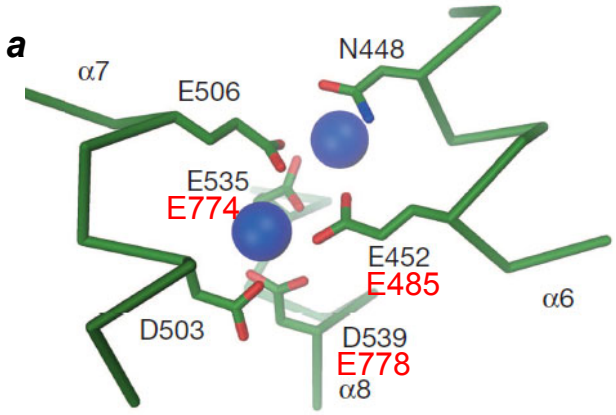

Dutzler et al., Nature 2014

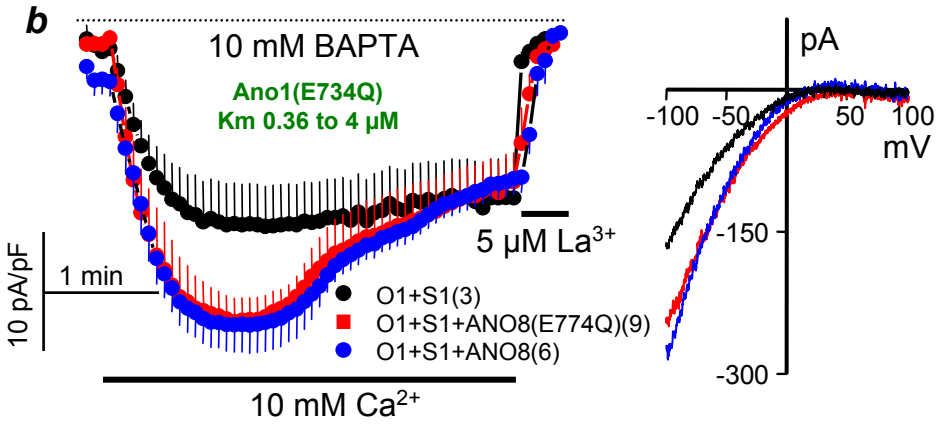

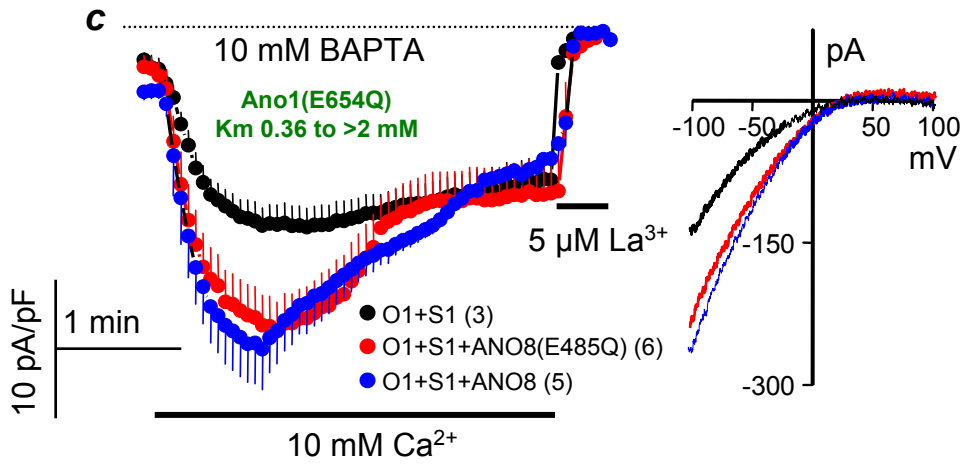

Figure EV8, Jha et al.

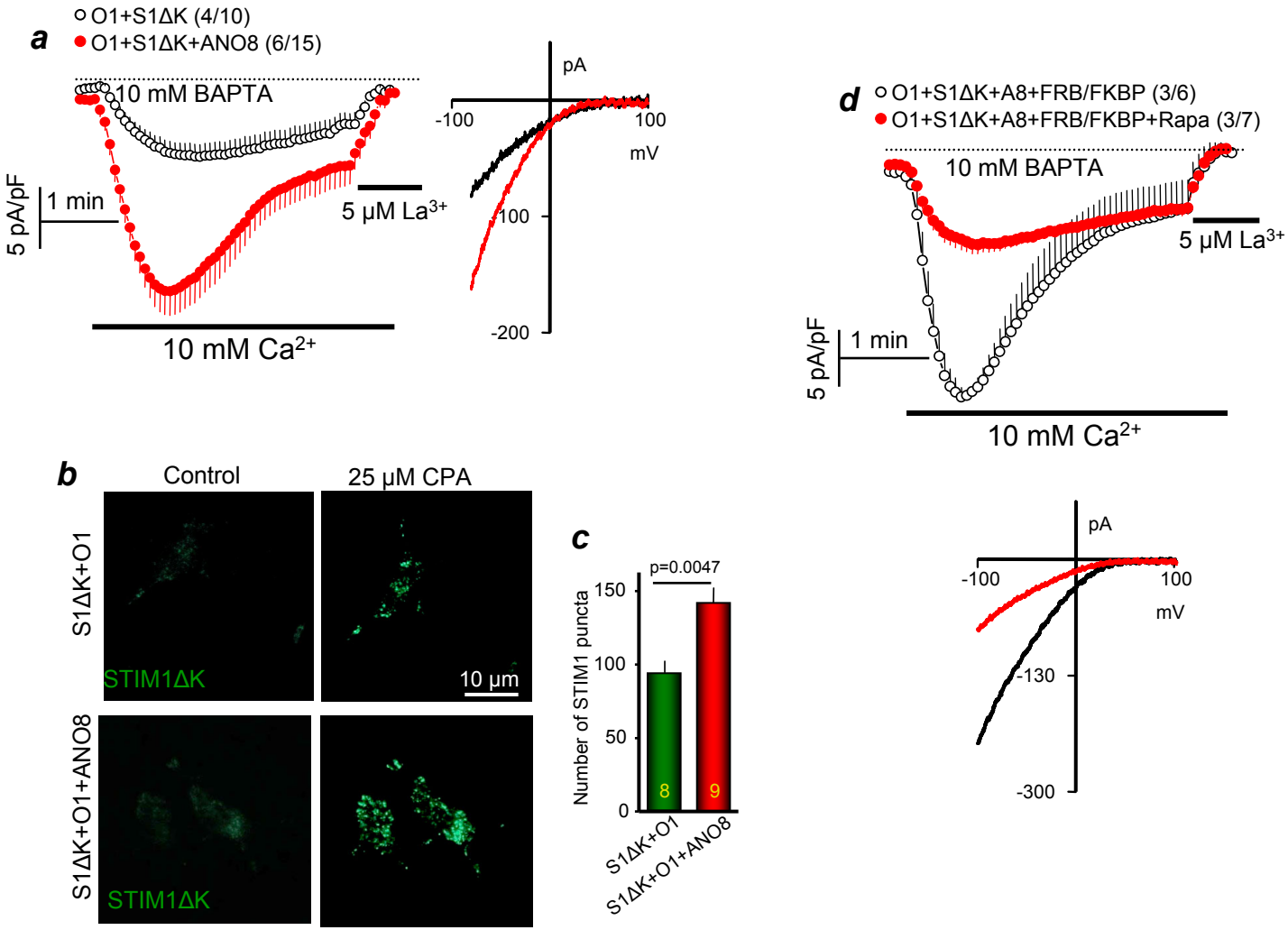

Figure EV9, Jha et al.

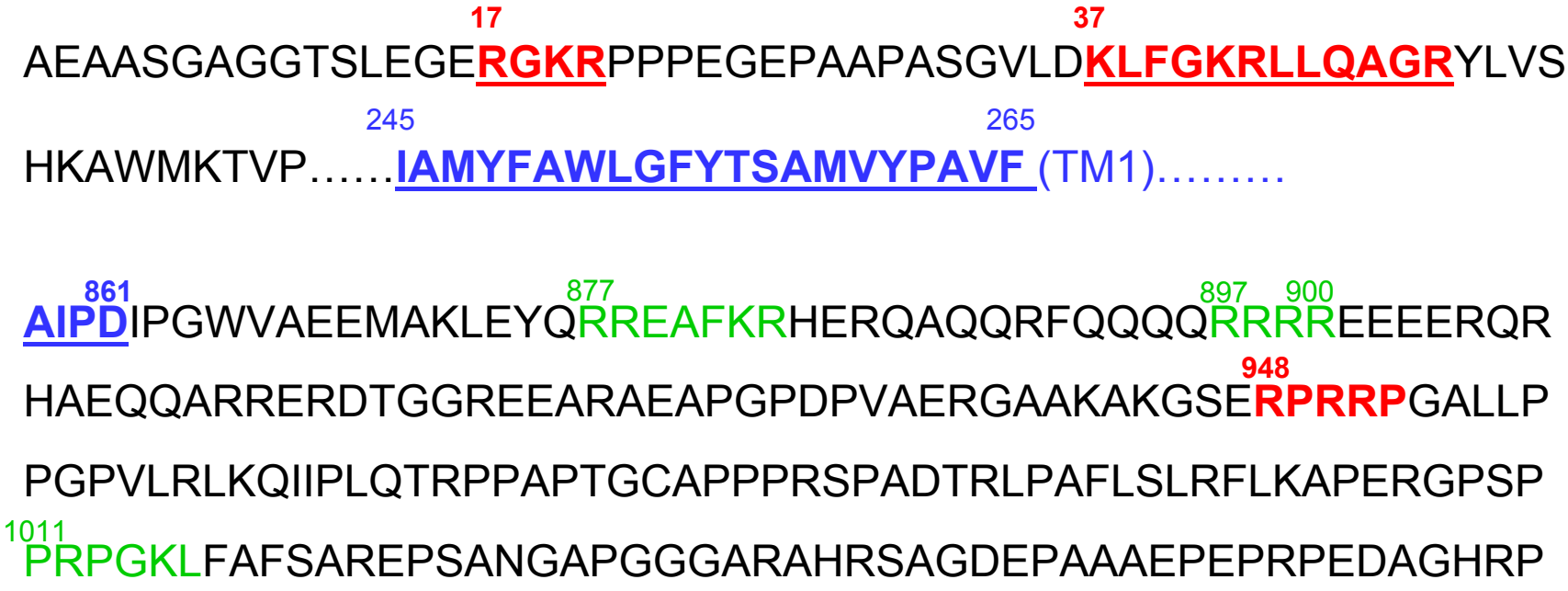

Figure EV10, Jha et al.

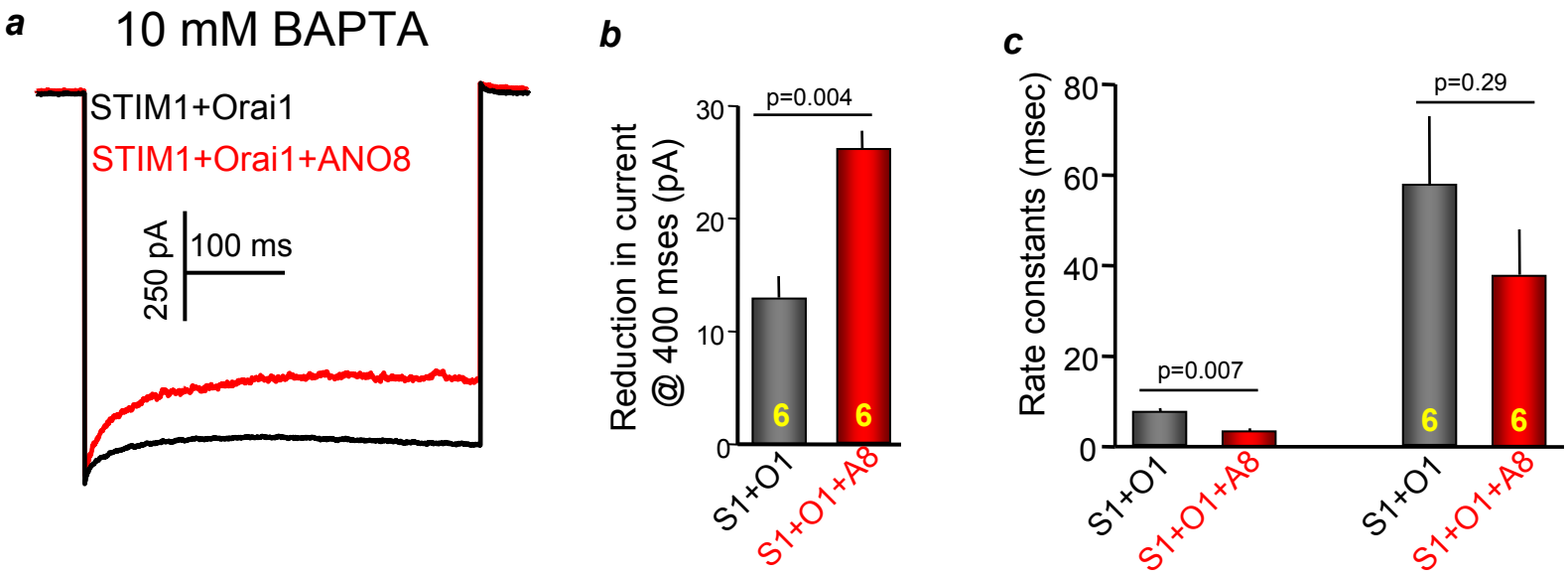

Table EV1: List of siRNAs used in the present study.

Construct	Primers	% knockdown
siANO1	rCrGrGrGrUrCrUrCrArUrUrArArUrGrUrGrGrUrArCrArUrCrUrUrC rArGrArUrGrUrArCrCrArCrArUrUrArArUrGrArGrArCrCCG	85
siANO2	rUrArGrCrArGrCrUrUrCrCrUrGrUrCrArUrUrCrArUrArUrCrGrUrC rCrGrArUrArUrGrArArUrGrArCrArGrGrArArGrCrUrGrCTA	93
siANO3	rUrCrUrArCrCrCrArUrArCrArUrUrUrArCrUrUrCrArGrCrUrCrUrUrC rArGrArArGrCrUrGrArArGrUrArArArUrGrUrArUrGrGrUrAGA	60
siANO4	rArArCrCrUrGrCrUrUrArUrUrUrGrUrUrUrArUrCrGrArUrCrCrUrG rGrGrArUrCrGrArUrArArArCrArArArUrArArGrCrArGrGTT	72
siANO5	rUrArGrArGrUrUrUrArGrCrArGrUrCrUrUrUrCrArArUrCrCrCrArA rGrGrGrArUrUrGrArArArGrArCrUrGrCrUrArArArCrUrCTA	65
siANO6	rGrArCrArGrArUrArArGrGrUrUrArGrArUrUrCrGrUrArUrUrGrCrUrU rGrCrArUrArCrGrArArUrCrUrArArCrCrUrUrArUrCrUrGTC	67
siANO8	rGrUrGrGrArGrArGrCrGrArGrCrUrArCrGrCrUrUrCrUrUCA rUrGrArArGrArArGrCrGrUrArGrCrUrCrGrCrUrCrUrCrCrArCrArU	91
siANO9	rGrCrUrGrArArGrArArGrGrCrArArCrUrCrUrArCrUGT rArCrArGrUrArGrArGrUrUrGrCrCrUrUrCrUrUrUrCrArGrGrCrArU	62
siANO10	rCrUrArGrUrArArCrArUrUrCrUrArArUrCrUrUrGrGrArGrGrCrArC rGrCrCrUrCrCrArArGrArUrUrArGrArArUrGrUrUrArCrUAG	70
siSARAF	rCrCrArGrGrArGrArCrGrArUrArArArGrUrArGrArArArGrTrT rCrCrArGrGrArGrArCrGrArUrArArArGrUrArGrArArArGrTrT	91
Scrambled	rCrGrUrArArUrCrGrCrGrUrArArUrArCrGrCrGrUrArT- rArUrArCrGrCrGrUrArUrUrArCrGrCrGrArUrUrArArCrGrArC	0

Table EV2: List of primers used in the present study.

R948,950,951Q	F: 5’ GCCAAGGCCAAGGGCAGCGAGCAGCCCCAACAGCCCGGAGCGCTGCTG CCACCC 3’ R: 5’ GGGTGGCAGCAGCGCTCCGGGCTGTTGGGGCTGCTCGCTGCCCTTGGCCTTGGC 3’
ANO8 E485Q	F: 5’ CAGCTGCTGCAGAACGTGCGCGCGGTGCTGCAGCCGCACCTGTAC 3’ R: 5’ GTACAGGTGCGGCTGCAGCACCGCGCGCACGTTCTGCAGCAGCTG 3’
ANO8 E774Q	F: 5’ GCCCTCGTCAACAACCTGATTCAGATCCGAAGTGATGCCTTCAAG 3’ R: 5’ CTTGAAGGCATCACTTCGGATCTGAATCAGGTTGTTGACGAGGGC 3’